

# The correlations between optical variability and physical parameters of quasars in SDSS Stripe 82

Wenwen Zuo, Xue-Bing Wu, Yi-Qing Liu, & Cheng-Liang Jiao  
Department of Astronomy, Peking University, Beijing 100871, China

## ABSTRACT

We investigate the optical variability of 7658 quasars from SDSS Stripe 82. Taking advantage of a larger sample and relatively more data points for each quasar, we estimate variability amplitudes and divide the sample into small bins of redshift, rest-frame wavelength, black hole mass, Eddington ratio and bolometric luminosity respectively, to investigate the relationships between variability and these parameters. An anti-correlation between variability and rest-frame wavelength is found. The variability amplitude of radio-quiet quasars shows almost no cosmological evolution, but that of radio-loud ones may weakly anti-correlate with redshift. In addition, variability increases as either luminosity or Eddington ratio decreases. However, the relationship between variability and black hole mass is uncertain; it is negative when the influence of Eddington ratio is excluded, but positive when the influence of luminosity is excluded. The intrinsic distribution of variability amplitudes for radio-loud and radio-quiet quasars are different. Both radio-loud and radio-quiet quasars exhibit a bluer-when-brighter chromatism. Assuming that quasar variability is caused by variations of accretion rate, the Shakura-Sunyaev disk model can reproduce the tendencies of observed correlations between variability and rest-frame wavelength, luminosity as well as Eddington ratio, supporting that changes of accretion rate plays an important role in producing the observed optical variability. However, the predicted positive correlation between variability and black hole mass seems to be inconsistent with the observed negative correlation between them in small bins of Eddington ratio, which suggests that other physical mechanisms may still need to be considered in modifying the simple accretion disk model.

*Subject headings:* galaxies: active — galaxies: nuclei — quasars: general — quasars: variability

## 1. Introduction

Variability is one of the major characteristics of Active Galactic Nuclei (AGNs), whose luminosities vary in all the bands from  $\gamma$ -ray to radio, on timescales from hours to years. Although the study of variability plays an important role in investigating the nature of the compact central region in AGNs (Hook et al. 1994; Wilhite et al. 2008), the mechanism underlying quasar variability is still inconclusive. Several physical mechanisms have been proposed to explain quasar variability (Vanden Berk et al. 2004), including accretion disk instabilities (Rees 1984; Kawaguchi et al. 1998; Kato et al. 1996; Manmoto et al. 1996; Czerny et al. 2008), Poissonian processes, such as multiple supernovae or star collisions (Terlevich et al. 1992; Courvoisier et al. 1996; Torricelli-Ciamponi et al. 2000), and gravitational microlensing (Hawkins 1993).

To clarify the nature of quasar variability, most previous studies focused on the dependencies of the variability indicator on redshift, time lag, rest-frame wavelength and luminosity. A decrease of variability was found towards longer wavelengths (Cutri et al. 1985; Paltani & Courvoisier 1994; di Clemente et al. 1996), but the influences of other parameters on the correlation were not excluded due to small samples. Vanden Berk et al. (2004) confirmed such an anti-correlation by excluding the dependencies of variability on redshift and luminosity, however, for the scarcity of data points of each quasar, they estimated one variability indicator from a sample of quasars (the ensemble variability method) rather than from an individual quasar (the individual variability method). This ignores the diversity of an individual quasar light curve, which may eventually fade out the actual relations. Due to the statistical incompleteness of small samples, previous studies found controversial evidences for the dependencies of variability on redshift and luminosity (Bonoli et al. 1979; Netzer & Sheffer 1983; Cristiani et al. 1990; Giallongo et al. 1991; Hook et al. 1994). Thus, the results may not be statistically reliable due to possible dependencies of variability on other parameters. Only recently, with larger samples, some work managed to disentangle the anti-correlation between the variability amplitude and luminosity by restricting other parameters in small ranges (Wilhite et al. 2008; Bauer et al. 2009). However, they still adopted the ensemble variability method to estimate the variability indicator. Moreover, as Wilhite et al. (2008) only studied quasars with redshift larger than 1.69, the situation for quasars with lower redshifts were still unknown. Besides luminosity, more attention has been paid to investigate the influences on variability from other intrinsic parameters, i.e., black hole mass and Eddington ratio (the ratio of bolometric luminosity to Eddington luminosity). Wold et al. (2007) found a correlation between variability and black hole mass from about 100 quasars, without accounting for the influences of other parameters. Based on their ensemble variability study of nearly 23,000 quasars from the Palomar QUEST Survey, Bauer et al. (2009) found the dependencies of quasar variability on black hole mass

(positively), and Eddington ratio (negatively). Similar conclusions were reached by Ai et al. (2010) based on the individual variability indicators but without disentangling the relations between these parameters.

Although variability depends on many parameters, the underlying physical mechanisms are still uncertain. Dividing the sample according to different parameter bins is essential to analyze their influences on variability. Moreover, to avoid missing the diversity of the individual quasar light curve, the detailed variability indicator of each quasar rather than the ensemble variability indicator from a group of quasars, should also be utilized. However, no previous work has employed the two essential methods simultaneously in their correlation analysis.

In this paper we revisit the correlations between the variability amplitude and physical parameters based on a sample of 7658 quasars in SDSS Stripe 82, with both the individual variability method and the detailed parameter binning techniques. We describe the sample selection and quasar variability estimations in § 2. The variability distribution and color-brightness relationship are given in § 3. § 4 shows the correlation between the variability amplitude and rest-frame wavelength for radio-loud and radio-quiet quasars. § 5 shows the correlation between variability and redshift. We disentangle the dependencies of variability on Eddington ratio, luminosity and black hole mass in § 6. Implications of our results and the comparison with the accretion disk model are presented in § 7. We summarize our results in § 8. The cosmological parameters of  $(h_0, \Omega_0, \lambda_0)$  are set to be (0.73, 0.27, 0.73) throughout the paper.

## 2. Quasar sample and variability estimation

### 2.1. Sample

A sample of 9254 variable quasars is obtained from cross-matching the spectroscopic confirmed SDSS DR7 quasars (Schneider et al. 2010; Shen et al. 2011) and a sample of 67507 variable sources in SDSS Stripe 82, which lies along the celestial equator in the Southern Galactic Hemisphere ( $22^{\text{h}} 24^{\text{m}} < \alpha_{J2000} < 04^{\text{h}} 08^{\text{m}}$ ,  $-1.27^\circ < \delta_{J2000} < +1.27^\circ$ ,  $\sim 290 \text{ deg}^2$ ) and have repeated photometric observations (at least 4 per band, with a median of 10) measured in up to 10 years in the  $u'g'r'i'z'$  system (Fukugita et al. 1996; MacLeod et al. 2010; Ivezić et al. 2007; Sesar et al. 2007). Black hole masses, bolometric luminosities and Eddington ratios are obtained from the quasar catalog in Shen et al. (2011), where the black hole masses of quasars were settled by fiducial virial mass estimates:  $\text{H}\beta$  (Vestergaard & Wilkes 2006) estimates for  $z < 0.7$ ,  $[\text{MgII}]$  (Shen & Kelly 2010) estimates for  $0.7 \leq z < 1.9$  and

CIV] (Vestergaard & Wilkes 2006) estimates for  $z \geq 1.9$ . If more than one emission line are available, we still adopt the fiducial virial black hole mass in Shen & Kelly (2010). In total, the quantity is measurable for 9148 quasars (98.9%) in the sample.

## 2.2. Variability estimation

To measure the variability amplitude in each filter band for each quasar, we adopt the formalism similar to that used in Ai et al. (2010) and Sesar et al. (2007):

$$\Sigma = \sqrt{\frac{1}{n-1} \sum_{i=1}^n (m_i - \langle m \rangle)^2} \quad (1)$$

$$V = \begin{cases} (\Sigma^2 - \xi^2)^{1/2}, & \text{if } \Sigma > \xi, \\ 0, & \text{otherwise.} \end{cases} \quad (2)$$

where  $n$  is the number of observations for a single source in each band,  $m_i$  is the magnitude from the  $i_{\text{th}}$  observation,  $\langle m \rangle$  is the mean magnitude, and  $\xi$  is estimated from the photometric error  $\Delta m_i$ :

$$\xi^2 = \frac{1}{n} \sum_{i=1}^n (\Delta m_i)^2 \quad (3)$$

We adopt  $V$  calculated in this way as the variability amplitude, which describes the intrinsic quasar variability by excluding the photometric error. Before estimating the variability amplitude in one band for an individual quasar, we eliminate the photometric outliers to make sure the calculated variability amplitude is not caused by non-physical reasons (Schmidt et al. 2010; MacLeod et al. 2010; Butler & Bloom 2011). Assuming that a significant decrease in magnitude in a single observation may be non-physical (Schmidt et al. 2010), we exclude data points with very faint luminosity, i.e., magnitude fainter than 30. Data points with large photometric uncertainties (errors larger than 1 magnitude) are also excluded. Photometric measurements are marked as outliers if the residuals between them and their median magnitude of all the preliminarily cleaned data points are above 5 times their standard deviation. This procedure is iterated until all the outliers are excluded, each time removing only the strongest outlier and updating the median magnitude along with the standard deviation for the remaining measurements. After eliminating all the assumed non-physical outliers, if more than 10 cleaned data points remained, we calculate the variability amplitude with the equations mentioned above. Otherwise, variability amplitudes are set to be 0. To get more reliable statistical results, in the following studies we only investigate

quasar variability amplitudes in the SDSS  $g'$ ,  $r'$  and  $i'$  band, as photometric errors in the  $u'$  and  $z'$  band are substantially larger (Sesar et al. 2007). Among the 9148 quasars with measurable black hole mass (Shen & Kelly 2010), 8967 quasars have reliable variability indicators in the  $g'$ ,  $r'$  and  $i'$  band, which means that variability in each band for a quasar is a non-zero value estimated from at least 10 data points, even after eliminating photometric outliers.

### 3. Variability distribution and color changes

Since the physical origin of optical variability in radio-quiet and radio-loud quasars may be different (Giveon et al. 1999), among the 8967 quasars, we divide the 7658 quasars with either radio detections or in the fields of the FIRST radio survey into two subsamples (White et al. 1997): the radio-quiet subsample contains quasars with radio loudness below 10; the radio-loud subsample holds quasars with radio loudness above 10. Here radio loudness is defined as the ratio of the observed radio flux density at rest-frame 6 cm and the optical flux density at rest-frame 2500 Å (Becker et al. 1995; Shen et al. 2011). 416 radio-loud sources and 7242 radio-quiet sources are obtained for the study in the following sections.

From Fig. 1, we can see that the variability amplitudes of the radio-quiet and the radio-loud quasars are mostly distributed between 0.05 mag and 0.3 mag, except that there is a relatively higher fraction of the radio-loud quasars ( $\sim 2.96\%$ ) with variability amplitudes larger than 0.3 mag compared to that of the radio-quiet quasars ( $\sim 1.73\%$ ). The median variability amplitude of the radio-quiet objects in the  $g'$ ,  $r'$  and  $i'$  band are  $0.125 \pm 0.071$  mag,  $0.106 \pm 0.060$  mag and  $0.095 \pm 0.057$  mag and that of the radio-loud objects are  $0.127 \pm 0.096$  mag,  $0.106 \pm 0.081$  mag and  $0.096 \pm 0.078$  mag respectively. Therefore, the median variability amplitude of the radio-quiet objects is very similar compared to that of the radio-loud quasars. However, their distributions differ significantly according to the results of 100 Kolmogorov-Smirnov (KS) tests (the median  $p \sim 0.012$ ). Each time we randomly split both the radio-quiet and radio-loud quasar samples into half and perform KS tests on the generated samples. For variability values in the  $g'$ ,  $r'$  and  $i'$  band, 99.7, 91.7 and 81.5 percent of p values from these KS tests are less than 0.05 respectively, further indicating significant differences between their intrinsic distributions. Moreover, for both these radio-quiet and radio-loud quasars, the median variability amplitude decreases systematically as the observed wavelengths increase (see § 4 for more details).

Here we take the magnitude difference between two adjacent SDSS filter bands as the color indicator. Using the data in the  $g'$ ,  $r'$  and  $i'$  filter band, we can get 2 colors, namely  $g'-r'$  and  $r'-i'$ . If both the difference of time in which the quasar luminosity of two adjacent

bands show their brightest state and the difference of time when luminosity of two adjacent bands show their faintest state are less than 2 days, then these quasars are selected to study the quasar color behavior. For the color  $g'-r'$  and  $r'-i'$ , we find 2811, 2553 radio-quiet quasars and 166, 158 radio-loud ones respectively. The differences between colors in the brightest state and faintest state are shown in Fig. 2. Both the radio-quiet and radio-loud quasars display a strong bluer-when-brighter chromatism; namely 82.9%, 67.8% of the radio-quiet quasars and 77.1%, 63.3% of the radio-loud quasars become bluer in the  $g'-r'$  and  $r'-i'$  color respectively, when they become brighter.

#### 4. Dependence on the rest-frame wavelength

As quasar variability amplitudes depend on quasar bolometric luminosity ( $L_{\text{bol}}$ ), rest-frame wavelength ( $\lambda_{\text{rf}}$ ), black hole mass ( $M_{\text{BH}}$ ) and possibly redshift ( $z$ ), such dependencies can be formulated as  $V(\lambda_{\text{rf}}, z, M_{\text{BH}}, L_{\text{bol}})$ , where the combination of dependencies of the variability amplitude on  $M_{\text{BH}}$  and  $L_{\text{bol}}$  can be replaced by the combination of its dependencies on  $M_{\text{BH}}$  and  $R_{\text{EDD}}$  (Eddington ratio) or that on  $R_{\text{EDD}}$  and  $L_{\text{bol}}$ . Dependencies of the variability amplitudes on each parameter can be obtained in subsamples where other parameters are constrained within small ranges. Some subsamples or sub-subsamples obtained from the combinations of those parameters yield unphysical (imaginary) correlation results. In most cases when this occurs the number of quasars is less than 10. In order to obtain statistically significant results, we require at least 10 quasars in a data set before including it in the analysis. For all further analysis, binned data sets including fewer than 10 quasars are rejected. The bin size of  $z$  is 0.3 and that of  $R_{\text{EDD}}$ ,  $M_{\text{BH}}$  and  $L_{\text{bol}}$  are all 0.5 dex. The minimum values of the four parameters are respectively 0.08,  $10^{7.0} M_{\odot}$ ,  $10^{44.3} \text{erg/s}$  and  $10^{-3.13}$ , while the maximum values are 5.08,  $10^{10.8} M_{\odot}$ ,  $10^{48.0} \text{erg/s}$  and  $10^{0.7}$ . In this work, the ranges of the four parameters are chosen to be  $[0.08, 4.9]$ ,  $[10^{7.5} M_{\odot}, 10^{10.5} M_{\odot}]$ ,  $[10^{44.5} \text{erg/s}, 10^{48.0} \text{erg/s}]$  and  $[10^{-2.0}, 10^{0.5}]$  respectively, as shown in Table 1. More than 99.5 percent of quasars can be covered in this way and further expansion of the ranges does not yield more qualified subsamples. Supposing that  $X$  is one of the five parameters ( $\lambda_{\text{rf}}$ ,  $z$ ,  $M_{\text{BH}}$ ,  $L_{\text{bol}}$  and  $R_{\text{EDD}}$ ), Spearman's Correlation Coefficient  $r_{1-X}$  is calculated in each corresponding subsample or sub-subsample to describe the rank correlation, while the significance  $p_{-X}$  of its value deviating away from 0 is also obtained. To parameterize the observed relation between the variability amplitude and the parameter  $X$ , we fit all the data in each subsample with a simple function:

$$V(X) = b_{-X} \log X + a_{-X} \tag{4}$$

Accompanied by the slope  $b_{\log X}$  and y axis intercept value  $a_{\log X}$ , Pearson Product-Moment Correlation Coefficient  $r_{2_{\log X}}$  is also calculated to illustrate the strength of the proposed relation ( $r_{2_{\log X}}$  for short). In the following sections,  $X$  will be replaced with  $\lambda_{\text{rf}}$ ,  $z$ ,  $M_{\text{BH}}$ ,  $L_{\text{bol}}$  and  $R_{\text{EDD}}$ .

To isolate the dependence of the variability amplitude on rest-frame wavelength for the radio-quiet quasars, we first divide the 7242 radio-quiet quasars into small bins in a two-dimensional space of redshift and Eddington ratio, as shown in Fig. 3. Ranging from the minimum value to the maximum value,  $z$  is divided into 16 bins.  $\log R_{\text{EDD}}$  is divided into 5 bins, as listed in Table 1. This procedure yields  $16 \times 5$  possible subsamples. Each subsample is further divided in 6  $\log M_{\text{BH}}$  bins. As seen in Fig. 3, 49 subsamples containing more than 10 quasars in each, which are filled with red points, are further subdivided in  $\log M_{\text{BH}}$ . The indices of the 49 qualified subsamples are shown in the lower corner of the corresponding grids. 104 qualified sub-subsamples with more than 10 quasars in each are finally constructed, e.g., indices like 1\_(1-2) means that 2 qualified sub-subsamples are selected from 6 small bins after the division of  $\log M_{\text{BH}}$  of the subsample ( $0.08 < z \leq 0.4$  and  $-1.5 < \log R_{\text{EDD}} \leq -1.0$ ). We calculate  $r_{1_{\lambda_{\text{rf}}}}$ ,  $r_{2_{\lambda_{\text{rf}}}}$  and fit all the data in each qualified sub-subsample with the function like Eq. (4).

To demonstrate the rest-frame wavelength  $\lambda_{\text{rf}}$  dependence of the variability amplitude  $V$  with significant statistics, in Fig. 4 we show the results of the 25 sub-subsamples containing the most numerous quasars, starting with the largest sub-subsample. To make the relation more obvious in each panel,  $\lambda_{\text{rf}}$  of the qualified sub-subsample is evenly divided into 10 bins. The median variability in each bin is denoted as red diamonds. Error bars show the standard deviation of variability values for quasars in each rest-frame wavelength bin. For the radio-loud quasars, we utilize the same mechanism to investigate the relationship between  $V$  and  $\lambda_{\text{rf}}$ . 8 qualified sub-subsamples are obtained from binning the 416 radio-loud quasars in  $\log R_{\text{EDD}}$ ,  $z$  and  $\log M_{\text{BH}}$ . The ranges of these binned parameters and the correlations between  $V$  and  $\lambda_{\text{rf}}$  are shown in Fig. 21 in the Appendix. Note that for radio-loud quasars, figures like Fig. 21, which describe the dependencies of variability on the quasar parameters will be shown in the Appendix. For both these radio-quiet and radio-loud quasars, the anti-correlation between  $V$  and  $\lambda_{\text{rf}}$  is evident —quasars appear to be less variable at larger rest-frame wavelengths. It is further confirmed by the distributions of calculated  $r_{1_{\lambda_{\text{rf}}}}$ ,  $r_{2_{\lambda_{\text{rf}}}}$ ,  $b_{\lambda_{\text{rf}}}$  and  $b_{\text{err}_{\lambda_{\text{rf}}}}$  values, as shown in Fig. 5. In the left panel, the dots on the left of  $r_{1_{\lambda_{\text{rf}}}} = 0$  suggest that the majority of the qualified radio-quiet sub-subsamples exhibit negative  $r_{1_{\lambda_{\text{rf}}}}$ , with a median value of -0.229. The significance  $p_{\lambda_{\text{rf}}}$  of its value deviation away from 0 is 0.019, which confirms the moderate anti-correlation at a confidence level over 98%, while the distribution of the asterisk signs presents that the median  $r_{1_{\lambda_{\text{rf}}}}$  value for all the 8 radio-loud sub-subsamples is -0.187 with a lower significance level ( $p \sim 0.218$ ). In the



middle panel,  $r2_{\lambda_{\text{rf}}}$  values for the 100 radio-quiet and all the 8 radio-loud sub-samples are smaller than 0. The median values are -0.233 and -0.224 for the radio-quiet and the radio-loud data sets respectively, while the distribution of the radio-quiet quasars is broader than the radio-loud data sets. From the fitting procedure, the median values of  $b_{\lambda_{\text{rf}}}$  and  $a_{\lambda_{\text{rf}}}$  for the radio-quiet sub-samples are  $-0.137 \pm 0.052$  and  $0.579 \pm 0.180$ , while the median  $b_{\lambda_{\text{rf}}}$  and  $a_{\lambda_{\text{rf}}}$  value for the radio-loud sub-samples are  $-0.225 \pm 0.143$  and  $0.950 \pm 0.494$ . The relative ratios of  $b_{\lambda_{\text{rf}}}$  and their errors  $b_{\text{err}}_{\lambda_{\text{rf}}}$  are shown in the right panel, where the ratios are generally larger for these radio-quiet sub-samples, implying a more robust linear relation.

## 5. Dependence on redshift

We first exclude the influences of the intrinsic quasar parameters on the variability amplitude by dividing the radio-quiet and radio-loud quasar sample into small bins in the  $\log M_{\text{BH}}\text{-}\log R_{\text{EDD}}$  space with their bin sizes of 0.5 dex. For radio-quiet quasars, 23 subsamples are considered qualified, with more than 10 quasars in each one. As shown in Fig. 6, 23 grids marked with algebraic numbers in the lower side of the grids and filled with red points refer to those qualified subsamples. For the radio-loud quasars, only 11 subsamples are qualified. To eliminate the influence of rest-frame wavelength on the relation between the variability amplitude and redshift, we prefer to divide  $\lambda_{\text{rf}}$  into small bins. However, as the rest-frame wavelength and redshift are closely related, the binning of  $\lambda_{\text{rf}}$  in one individual SDSS filter band will lead to a decrease of the redshift range, causing the evaluated dependence of variability on redshift unreliable (Vanden Berk et al. 2004). Therefore, we treat variability amplitudes in the 3 bands ( $g'$ ,  $r'$  and  $i'$ ) for an individual quasar as variability amplitudes for 3 individual quasars with the same redshift. Based on the variability amplitude and  $\lambda_{\text{rf}}$  of the triple-enlarged subsample, we choose an intersecting range of  $\lambda_{\text{rf}}$  in the 3 bands for quasars in each qualified subsample, which are binned with an equal size of 400 Å. In this way, we manage to exclude the influence of  $\lambda_{\text{rf}}$  on the correlation between  $V$  and  $z$  by restricting the sub-sample in small ranges of rest-frame wavelength, but without decreasing the range of  $z$ . We use the same method mentioned in § 4 to select qualified sub-samples, e.g., indices like 1-(1-4) in Fig. 6 means that after the  $\lambda_{\text{rf}}$  division of the subsample ( $10^{7.5} M_{\odot} < M_{\text{BH}} \leq 10^8 M_{\odot}$  and  $-1 < \log R_{\text{EDD}} \leq -0.5$ ) into several sub-samples, 4 of them are qualified with more than 10 quasars in each. The ranges of  $M_{\text{BH}}$  and  $R_{\text{EDD}}$  for each sub-sample are shown in Fig. 6 and the range of  $\lambda_{\text{rf}}$  is shown further in the lower right of each panel in Fig. 7.

The relation between the variability amplitude and redshift for the 25 qualified radio-



quiet sub-samples containing the largest numbers of quasars are shown in Fig. 7, including the values of  $r_{1-z}$ ,  $r_{2-z}$ ,  $b_{-z}$  and the ranges for all the restricted parameters. We evenly separate the quasars into 10 redshift bins, to make these tendencies more obviously seen. The median variability amplitude  $V$  and redshift  $z$  in each bin are denoted as red diamonds, and error bars show the dispersion of variability values for these quasars. These results are fairly noisy, and it is difficult to detect any clear trend with redshift, which is further confirmed in Fig. 8. Again in a similar way, the 11 qualified radio-loud subsamples are divided into sub-samples with a bin size of rest-frame wavelength of 400 Å. 18 qualified sub-samples are obtained and details of their redshift dependence of variability are shown in Fig. 22 in the Appendix.

$r_{1-z}$ ,  $p_{-z}$ ,  $r_{2-z}$  and the results from the linear fitting for both the radio-quiet and radio-loud data sets are shown in Fig. 8. 78.3% of the radio-quiet sub-samples show negative  $r_{1-z}$  and  $r_{2-z}$  values. However, as 42.6% of the negative  $r_{1-z}$  values for the radio-quiet ones are close to zero within a range of 0.1, the median  $r_{1-z}$  value is -0.081 above 81.1% confidence level, suggesting almost no relation. Meanwhile, the middle panel indicates that no linear relation between them exists, consistent with the distribution of  $|b_{-z}|/|b_{\text{err}-z}|$  in the right panel—65.0% of these data sets show  $|b_{-z}|/|b_{\text{err}-z}|$  values less than 2. For the radio-loud data sets, 61.1 percent show negative relations; the median  $r_{1-z}$  value is -0.153 with the median confidence level ( $p_{-z} \sim 0.306$ ). The very weak negative relation has to be concerned with a larger radio-loud data set due to its low confidence level. Distributions of  $r_2$  and  $|b_{-z}|/|b_{\text{err}-z}|$  show no linear relation between them—55.6 percent of these sub-samples exhibit an anti-correlation between  $V$  and  $z$ , while the other ones show a positive relation.

## 6. Dependence on black hole mass, luminosity and Eddington ratio

Both the radio-quiet and radio-loud sample are first divided into 16 redshift bins as mentioned in § 4. For the 14 qualified subsamples of radio-quiet quasars with redshift ranging from 0.4 to 4.3 and 9 subsamples of the radio-loud quasars with redshift spanning from 0.4 to 3.1, we calculate Spearman’s Rank Correlation Coefficients between the variability amplitude in the 3 SDSS bands ( $g'$ ,  $r'$  and  $i'$ ) and the three intrinsic quasar parameters ( $M_{\text{BH}}$ ,  $L_{\text{bol}}$  and  $R_{\text{EDD}}$ ), without accounting for the relationships among the intrinsic quasar parameters themselves. Results for the radio-quiet and radio-loud quasar subsamples are shown as magenta diamonds and triangles in the left panel of Fig. 13, Fig. 16 and Fig. 19, respectively.

For both the radio-loud and radio-quiet subsamples, there is a weak anti-correlation between variability and  $R_{\text{EDD}}$  at a high confidence level. To make a distinction between

the Spearman’s Rank Correlation Coefficients here and  $r_1$  calculated after considering relationships among the intrinsic quasar parameters, we denote results here as the format like  $r_1^n\_X$ .  $r_1^n\_R_{\text{EDD}}$  of 12 radio-quiet and all the radio-loud subsamples are less than 0 and the median values for these radio-quiet and radio-loud subsamples are approximately -0.170 and -0.390 respectively. Most of the  $p^n\_R_{\text{EDD}}$  values are around 0. A weak anti-correlation between the variability amplitude and  $L_{\text{bol}}$  shows up as more than 90% subsamples exhibit negative  $r_1^n\_L_{\text{bol}}$  values at a confidence level over 99%. The median  $r_1^n\_L_{\text{bol}}$  values for the radio-quiet and the radio-loud subsamples are -0.290 and -0.350 respectively. However, no conclusive results are found for the relation with  $M_{\text{BH}}$ . This is consistent with the anti-correlation between variability and  $L_{\text{bol}}$  found in previous studies on smaller samples, where the relations among the intrinsic quasar parameters were not taken into consideration either (Cristiani et al. 1996; di Clemente et al. 1996; Paltani & Courvoisier 1997). The correlation between variability and  $M_{\text{BH}}$  for the  $0.08 < z \leq 0.7$  radio-quiet sample ( $r_1^n\_M_{\text{BH}} \sim 0.26$ ,  $p^n\_M_{\text{BH}} \sim 0.01$  for the quasars within  $0.08 < z \leq 0.4$  and  $r_1^n\_M_{\text{BH}} \sim 0.13$ ,  $p^n\_M_{\text{BH}} \sim 0.01$  for the quasars within  $0.4 < z \leq 0.7$ ), corresponds well to the significant dependence of variability on  $M_{\text{BH}}$  for the  $0 < z < 0.75$  sample reported by Wold et al. (2007). We discuss this further in § 7.

However, the relations among the intrinsic quasar parameters have to be taken into account to investigate the influences of different parameters on the variability amplitude. As more luminous quasars tend to possess more massive black holes, the relationship between variability and black hole mass will also express itself in the correlation between variability and luminosity or the relation with Eddington ratio. As shown in this section, after considering the relationships among the intrinsic quasar parameters, trends are still clear in some cases but become ambiguous or fade out in other cases. The radio-quiet quasars and radio-loud quasars are subdivided into small data sets by binning redshift and one of the three quasar parameters to exclude their influences on the relationships between the variability amplitude and the other two quasar parameters. The separate consideration of variability amplitudes in the 3 filter bands manage to restrict the rest-frame wavelength of each data set to small ranges.

Fig. 3 shows the details of binning in the  $\log R_{\text{EDD}}-z$  space for the radio-quiet quasars and yields 49 qualified subsamples, as described in § 4. Fig. 9 and Fig. 10 show the details of binning in the  $\log M_{\text{BH}}-z$  space and  $\log L_{\text{bol}}-z$  space, respectively. In Fig. 9, among  $16 \times 6$  grids, 52 grids refer to the qualified subsamples. In Fig. 10,  $16 \times 7$  grids are obtained and 45 grids are qualified. For the radio-loud quasars, 11, 11 and 13 qualified subsamples are extracted in the  $\log R_{\text{EDD}}-z$ ,  $\log M_{\text{BH}}-z$  and  $\log L_{\text{bol}}-z$  spaces, respectively. In each qualified subsample, we further calculate  $r_1$ ,  $r_2$ ,  $b$  and  $a$  for the correlations between  $V$  and the other two unrestricted physical parameters. Their distributions are shown statistically in

Fig. 13, 16 and 19. For the subsamples obtained from binning in the  $\log R_{\text{EDD}}-z$  space, the corresponding signs (plus signs for results from the radio-quiet data sets and asterisk signs for results from the radio-loud data sets) are colored as red, while for the subsamples from binning in the  $\log M_{\text{BH}}-z$  and  $\log L_{\text{bol}}-z$  space, signs are colored as blue and grey respectively. Thus in the panels of Fig. 13, Fig. 16 and Fig. 19, which contain plus and asterisk signs, the number of red, blue and grey plus signs are  $49 \times 3$  (the  $g'$ ,  $r'$  and  $i'$  filter band),  $52 \times 3$  and  $45 \times 3$ , while the number of red, blue and grey asterisk signs are  $11 \times 3$ ,  $11 \times 3$  and  $13 \times 3$  respectively.

To demonstrate the dependence of the variability amplitude on  $L_{\text{bol}}$  in the qualified subsamples obtained from the  $\log R_{\text{EDD}}-z$  space and  $\log M_{\text{BH}}-z$  space, we further show the detailed relations for the 25 largest radio-quiet quasar data sets from the former space in Fig. 11 and that from the latter space in Fig. 12. To make these underlying tendencies more intuitively clear, in each subsample the unrestricted parameter  $L_{\text{bol}}$  on which we are studying the dependence of the variability amplitude, is further subdivided into 10 bins with an equal number of quasars in each one. The median variability amplitudes and median parameter values are shown as colored diamonds. The error bars represent the 68 percent dispersion of variability amplitudes for the quasars in each bin. Only in the  $r'$  band the variability amplitudes for all the quasars are further shown as grey points. The fitting of the linear relation between  $V$  and  $\log L_{\text{bol}}$  for all the data in each band are carried out, but only the resulting slope in the  $r'$  band is shown in the upper right of each panel.  $r1\_L_{\text{bol}}$ ,  $p\_L_{\text{bol}}$  and  $r2\_L_{\text{bol}}$  for the quasars in each subsample in the  $r'$  band are also listed. 94.0 percent of the two figures presents an evident anti-correlation between  $V$  and  $\log L_{\text{bol}}$ , consistent with the statistical study shown in Fig. 13.

As shown in Fig. 13, almost all subsamples exhibit an anti-correlation between the variability amplitude and  $L_{\text{bol}}$  after considering the relations among the intrinsic quasar parameters. The median value of  $r1\_L_{\text{bol}}$  for the radio-quiet subsamples within small ranges of  $z$  and  $\log R_{\text{EDD}}$  is  $-0.269$  over 98% confidence level, while the median value of  $r1\_L_{\text{bol}}$  for the radio-quiet subsamples within small ranges of  $z$  and  $\log M_{\text{BH}}$  is  $-0.343$  above 99% confidence level. The distribution of  $r2\_L_{\text{bol}}$  with a median value of  $-0.260$  and  $-0.335$  for the subsamples in the  $\log R_{\text{EDD}}-z$  space and  $\log M_{\text{BH}}-z$  space, respectively, as displayed in the middle panel, indicates a weak linear relation between  $V$  and  $\log L_{\text{bol}}$ . The distribution of the fitting slope  $b\_L_{\text{bol}}$  and its error is shown in the right panel. Based on the averaged value, the anti-correlation between the variability amplitude and  $L_{\text{bol}}$  can be described with a format similar to Eq. (4). The median values of  $b\_L_{\text{bol}}$  and  $a\_L_{\text{bol}}$  for the radio-quiet subsamples in the  $\log R_{\text{EDD}}-z$  space are  $-0.044 \pm 0.020$  and  $2.128 \pm 0.913$ , and for the radio-quiet subsamples in the  $\log M_{\text{BH}}-z$  space are  $-0.063 \pm 0.020$  and  $3.032 \pm 0.926$ . While for the radio-loud subsamples in the  $\log R_{\text{EDD}}-z$  space, the median  $r1\_L_{\text{bol}}$ ,  $r2\_L_{\text{bol}}$ ,  $b\_L_{\text{bol}}$  and

$a_{\text{bol}}$  are  $-0.266$  with a lower confidence level ( $p_{\text{bol}} \sim 0.297$ ),  $-0.269$ ,  $-0.058 \pm 0.054$  and  $2.794 \pm 2.456$ ; and in the  $\log M_{\text{BH}}-z$  space, the median  $r1_{\text{bol}}$ ,  $r2_{\text{bol}}$ ,  $b_{\text{bol}}$  and  $a_{\text{bol}}$  are  $-0.384$  with a significance of  $0.164$ ,  $-0.321$ ,  $-0.071 \pm 0.055$  and  $3.373 \pm 2.536$ . As displayed in the right panel, the error in  $b_{\text{bol}}$  is comparable to  $b_{\text{bol}}$  for the radio-loud quasars, indicating that the dispersion is large and the linear relation is very weak. According to the simplest Poissonian model, in which starburst events are independent and discrete, the luminosity variability is expected to vary with luminosity as  $\log V \propto 0.5 \log L_{\text{bol}}$  (Cid Fernandes et al. 2000). Despite the possibility that a wide range of  $b$  values could be obtained by considering more detailed Poissonian models, where supernovae and their remnants were considered,  $b$  is often close to  $-0.5$  (Vanden Berk et al. 2004; Paltani & Courvoisier 1997; Aretxaga et al. 1997). We fit our data with a two-parameter function  $\log V = b \log L_{\text{bol}} + a$  and the median  $b$  is  $-0.223 \pm 0.075$ . Thus, the results obtained from our sample does not support the Poissonian model.

The dependence of the variability amplitude on  $R_{\text{EDD}}$  is analyzed based on the 45 subsamples in the  $\log L_{\text{bol}}-z$  space and 52 qualified subsamples in the  $\log M_{\text{BH}}-z$  space. To specify the relation, the details for the 25 largest subsamples in each space are further shown in Fig. 14 and Fig. 15 respectively. Going from the upper to the lower panels within various parameter ranges in Fig. 15, the anti-correlation between  $V$  and  $R_{\text{EDD}}$  is apparent. While in only 4 panels of Fig. 14, we find no discernible relation or an insignificant correlation, such as the third panel in the lowest line.

Following the analysis of the relationship between variability and luminosity, statistical results of  $r1_{\text{EDD}}$ ,  $p_{\text{EDD}}$ ,  $r2_{\text{EDD}}$ ,  $b$  and  $|b_{\text{EDD}}|/|b_{\text{err-EDD}}|$  are shown in Fig. 16. For the radio-quiet quasars in the  $\log L_{\text{bol}}-z$  space and  $\log M_{\text{BH}}-z$  space, more than 80.0 percent and 94.2 percent of  $r1_{\text{EDD}}$  are negative respectively, indicating an anti-correlation between  $V$  and  $R_{\text{EDD}}$ . All the qualified radio-loud subsamples from the two spaces exhibit negative  $r1_{\text{EDD}}$  values. Respectively in the two spaces, the median  $r1_{\text{EDD}}$  value is  $-0.167$  ( $p_{\text{EDD}} \sim 0.137$ ) and  $-0.303$  ( $p_{\text{EDD}} \sim 0.013$ ) for the radio-quiet quasars; and  $-0.304$  and  $-0.369$  for the radio-loud quasars over a lower confidence level ( $p_{\text{EDD}} \sim 0.300$  and  $0.188$ ). As shown in the last 2 panels, 79.3% of the qualified radio-quiet subsamples obtained from the  $\log L_{\text{bol}}-z$  space exhibit negative  $r2_{\text{EDD}}$  and  $b_{\text{EDD}}$  values, confirming the weak anti-correlation between  $V$  and  $\log R_{\text{EDD}}$ . The linear relation for the qualified radio-quiet subsamples binned from the  $\log M_{\text{BH}}-z$  space is more evident with a median  $r2_{\text{EDD}}$  of  $-0.299$ . More than 92.3 percent of radio-loud subsamples from the  $\log L_{\text{bol}}-z$  space and all the qualified ones from the  $\log M_{\text{BH}}-z$  space display negative linear relations between  $V$  and  $\log R_{\text{EDD}}$ , with median  $r2_{\text{EDD}}$  values of  $-0.274$  and  $-0.291$  in the  $\log L_{\text{bol}}-z$  and  $\log M_{\text{BH}}-z$  space respectively. The linear relation is also described with a simple function like Eq. (4).  $|b_{\text{EDD}}|/|b_{\text{err-EDD}}|$  values are generally larger for the radio-quiet subsamples,

indicating a stronger linear relation. The median values of  $b_{R_{\text{EDD}}}$  and  $a_{R_{\text{EDD}}}$  for the radio-quiet subsamples in the  $\log L_{\text{bol}}-z$  space are  $-0.020 \pm 0.014$  and  $0.091 \pm 0.011$ , while for the radio-loud quasars the results become  $-0.045 \pm 0.032$  and  $0.079 \pm 0.035$  respectively. For the radio-quiet subsamples in the  $\log M_{\text{BH}}-z$  space the median values of  $b_{R_{\text{EDD}}}$  and  $a_{R_{\text{EDD}}}$  are  $-0.052 \pm 0.019$  and  $0.075 \pm 0.013$ ; for the radio-loud subsamples they are  $-0.069 \pm 0.047$  and  $0.056 \pm 0.055$ , respectively.

The relation between the variability amplitude and  $M_{\text{BH}}$  for the 25 largest qualified data sets obtained from binning in the  $\log R_{\text{EDD}}-z$  space is shown in Fig. 17, and that for the subsamples with restricted  $L_{\text{bol}}$  values is shown in Fig. 18. Almost all the subsamples in the former figure report an apparent inverse dependence of  $V$  on  $\log M_{\text{BH}}$ . Proceeding from the first panel to the last one in the latter figure, a positive relation is shown in general. Most subsamples show a significant positive  $\log M_{\text{BH}}$  dependence, especially for those containing more quasars (the first 8 panels). The opposite trend shown in some cases (such as the 3rd panel in the lowest line) is very weak and there are too few cases to claim deviations from the general trend.

The calculated  $r1_{M_{\text{BH}}}$ ,  $p_{M_{\text{BH}}}$ ,  $r2_{M_{\text{BH}}}$  and  $b_{M_{\text{BH}}}$  values for each subsample are shown in Fig. 19. In the subsamples obtained from binning in the  $\log R_{\text{EDD}}-z$  space, we can find that for both the radio-quiet and the radio-loud quasars, there is a significant anti-correlation between them with the median coefficient  $r1_{M_{\text{BH}}}$  about  $-0.203$  above 94% confidence level and  $-0.220$  at a lower confidence level ( $p_{M_{\text{BH}}} \sim 0.432$ ), respectively. While for the radio-quiet subsamples with  $L_{\text{bol}}$  limited, more than 71.1 percent show positive  $r1_{M_{\text{BH}}}$  values and its median value is  $0.113$  ( $p_{M_{\text{BH}}} \sim 0.235$ ); the median value of  $0.246$  ( $p_{M_{\text{BH}}} \sim 0.386$ ) is shown for the radio-loud quasars, suggesting an insignificant correlation. Based on the median values of the linear fitting results ( $b_{M_{\text{BH}}}$  and  $a_{M_{\text{BH}}}$ ), we can parameterize the relation between  $V$  and  $M_{\text{BH}}$  using Eq. (4) with  $X$  as  $\log M_{\text{BH}}$ , where  $b_{M_{\text{BH}}} = -0.033 \pm 0.019$  and  $a_{M_{\text{BH}}} = 0.394 \pm 0.168$  for the subsamples binned from the  $\log R_{\text{EDD}}-z$  space;  $b_{M_{\text{BH}}} = 0.013 \pm 0.014$  and  $a_{M_{\text{BH}}} = -0.002 \pm 0.119$  for the subsamples given by binning in the  $\log L_{\text{bol}}-z$  space. The median values of  $b_{M_{\text{BH}}}$  and  $a_{M_{\text{BH}}}$  are  $-0.052 \pm 0.052$ ,  $0.600 \pm 0.477$  in the  $\log R_{\text{EDD}}-z$  space and  $0.040 \pm 0.035$ ,  $-0.206 \pm 0.309$  in the  $\log L_{\text{bol}}-z$  space for the radio-loud quasars. It guarantees the information provided by the distribution of  $r1_{M_{\text{BH}}}$ —the relations are insignificant for the radio-loud subsamples. The median  $r1$ ,  $p$ ,  $r2$ ,  $b$ ,  $b_{\text{err}}$ ,  $a$  and  $a_{\text{err}}$  values for the relationships between  $V$  and different quasar parameters are all summarized in Table 2.

## 7. Discussion

### 7.1. Comparison with previous work

Vanden Berk et al. (2004) argued that variability of radio-loud quasars are larger than radio-quiet ones, while no evidence for a change in the average optical variability amplitude with increasing radio luminosity is shown in Bauer et al. (2009). Comparing the median variability amplitude, we do not find larger variability amplitudes for radio-loud quasars than radio-quiet ones. However, their intrinsic distributions are different based on the results of KS test. The variability of radio-loud quasars may be caused by some mechanisms other than the accretion disk instability, such as the outflow (Giveon et al. 1999).

We confirm the anti-correlation between the variability amplitude and rest-frame wavelength which is mostly studied in the form of ensemble structure functions (Cutri et al. 1985; Paltani & Courvoisier 1994; Vanden Berk et al. 2004). We show that both the radio-quiet quasars and radio-loud quasars exhibit a bluer-when-brighter chromatism, in good accordance with previous studies (Wilhite et al. 2005; Meusinger et al. 2010; Trèvese & Vagnetti 2001, 2002; Schmidt et al. 2012; Ai et al. 2011). Honma et al. (1991) showed that when instabilities occur in the inner disk, the integrated color will change because of the outward propagating hot wave, which can account for the bluer-when-brighter behavior. Sakata et al. (2011) also suggested that it may be caused by changes of accretion rate. Besides this explanation, radiations from different regions of accretion disk or influences of host galaxy may also induce such a behavior (Shields 1978; Malkan 1983; Hawkins 1993). However, as quasar optical luminosities are dominated by their disks rather than their host galaxies, accretion disk instabilities are more likely than influences of host galaxies to explain the bluer-when-brighter chromatism. Trevese & Vagnetti (2001, 2002) analyzed the dependence of spectral changes on the brightness of quasars and suggested that the chromatism is at least consistent with the temperature variation of a single emitting blackbody and can be explained by bright spots on the disk possibly produced by the accretion disk instability, which also agrees with Schmidt et al. (2012). It is also possible that a combination of these physical mechanisms produces the color chromatism.

We find no relation between the variability amplitude and redshift for radio-quiet quasars, which seems contrary to the negative or positive correlations reported in previous work (Cristiani et al. 1990; Hook et al. 1994; Trevese et al. 1994). The anti-correlation found in Cristiani et al. (1990) may reflect the anti-correlation between  $V$  and  $L_{\text{bol}}$ , as their sample is too small to disentangle the relation. Only Trevese et al. (1994) binned the magnitude limited sample within small luminosity and redshift ranges and found an anti-correlation, which is ascribed to the dependence of variability on wavelength. Some previous work



(Giveon et al. 1999; Schmidt et al. 2012) also found no relation between  $V$  and  $z$ . After correcting the contribution from emission lines, the color variability is independent of redshift (Schmidt et al. 2012), which agrees with our results. However, although Giveon et al. (1999) also found no relation between  $V$  and  $z$ , their conclusion is probably not reliable due to the small size and the narrow redshift range of the quasar sample. Our results do isolate the influences of rest-frame wavelength, black hole mass and Eddington ratio and suggest that the redshift dependence of radio-quiet quasar variability may not exist. The possible anti-correlation between  $V$  and  $z$  for radio-loud quasars is very weak and not significant; it may need to be investigated with a larger sample in the future.

By investigating the relationships between the variability amplitude and the intrinsic quasar parameters in different redshift ranges, both before and after binning in one of the parameters, we find some results that are different from those in previous work. In spite of obvious selection effects of the flux-limited sample within  $0 < z < 0.75$ , Wold et al. (2007) reported a significant dependence of variability on black hole mass, approximately 0.2 magnitude increase of the variability value over 2-3 orders of magnitude in black hole mass. They used the maximum magnitude difference of light curves as the variability indicator, which is approximately 4 times larger than our estimated variability value. Before considering the relations among the intrinsic quasar parameters, the quasars within  $0.08 < z \leq 0.4$  and  $0.4 < z \leq 0.7$  in our sample also show a relation between the quasar variability amplitude and black hole mass. However, this is not the whole story for the correlation between variability and  $M_{\text{BH}}$ . We do not find any certain relation between the variability amplitudes and black hole mass in the subsamples binned in the intrinsic quasar parameters. Most subsamples in narrow ranges of Eddington ratio exhibit a weak anti-correlation while the subsamples in narrow luminosity ranges show no relation or a weak correlation between variability values and black hole mass. We derived the best-fit parameters with the function similar to Eq. (10) in Bauer et al. (2009) for our subsamples in small bins of luminosity. Although the resulting slope for the largest subsample is  $0.067 \pm 0.018$ , from statistical results of all qualified radio-quiet samples we do not find the weak correlation stated in Bauer et al. (2009). The median slope is  $0.051 \pm 0.056$  compared to  $0.13 \pm 0.01$  in their work.

Wilhite et al. (2008) also found a correlation between the variability amplitude and black hole mass and an anti-correlation between the variability amplitude and luminosity independent of black hole mass. The black hole mass range of our sample ( $10^7 M_{\odot}$  -  $10^{10.8} M_{\odot}$ ) is larger than that of their sample, which makes our results statistically more significant. Compared to their results, the relation between the variability amplitude and luminosity is weaker in our case. This may be due to the fact that in our sample, many bright (faint) quasars also show large (small) variability, which further shallows the anti-correlation. Furthermore, this corresponds well to the anti-correlation found in small  $M_{\text{BH}}$  bins in Bauer et al. (2009),



where the logarithm value of the variability amplitude is proportional to  $(-0.205 \pm 0.002) \log L_{\text{bol}}$ . With our sample, we calculate the slope using the fitting function similar to theirs and the slope value is  $-0.263 \pm 0.074$ . We confirm the anti-correlation between variability and  $R_{\text{EDD}}$  (Wilhite et al. 2008; Ai et al. 2010) by excluding the influences of other parameters on the variability amplitude.

## 7.2. Implications of the standard accretion disk model

The optical continuum of low-redshift quasars can often be well fitted by the standard accretion-disk model proposed by Shakura & Sunyaev (1973). Following Li & Cao (2008), we investigate the dependencies of the variability amplitude on rest-frame wavelength and the intrinsic quasar parameters, assuming that quasar variability is caused by a change of accretion rate, which is the result of accretion disk instabilities. However, we do not utilize the temperature distribution shown in their work, as it is actually an approximation to the equatorial temperature in the outer region of the disk and depends on viscosity. The temperature distribution we used here describes the radial dependence of the effective temperature derived from the emergent flux from an accretion disk around a Schwarzschild black hole, which is independent of viscosity, namely,

$$T(R) = \left[ \frac{3GM\dot{M}}{8\pi\sigma R^3} \left( 1 - \sqrt{R_{\text{in}}/R} \right) \right]^{1/4}, \quad (5)$$

where  $R_{\text{in}} = 3R_g$ ,  $R_g = \frac{2GM}{c^2}$ . Here,  $\sigma$  is the Stefan-Boltzmann constant,  $R$  is the radius of the disk,  $M$  is the black hole mass,  $\dot{M}$  is the accretion rate. After calculating the emitting spectrum at each radius, we integrate it over the whole disk to get the final spectrum. The emitted spectrum of the disk can be written as:

$$f_\nu = \frac{4\pi h \cos(\beta) \nu^3}{c^2 D^2} \int_{R_{\text{in}}}^{R_{\text{out}}} \frac{R dR}{e^{h\nu/kT(R)} - 1}, \quad (6)$$

where  $R_{\text{out}}$  is the outer radius of the disk,  $h$  is Planck's constant,  $\beta$  is the inclination of the disk with respect to the line of sight and  $D$  is the luminosity distance from the observer to the quasar (Frank et al. 2002). We simply assume the inclination to be 0. It is a reasonable assumption since any inclination other than 0 will just reduce the normalization of the whole spectra, which does not affect the variability amplitude. In addition, the inclination is not likely to change significantly.

To better compare theoretical results with observations, we obtain  $\eta\dot{m}$  values in the model according to the representative  $R_{\text{EDD}}$  values in our sample.

$$\dot{M} = \dot{m}\dot{M}_{\text{crit}} = \eta\dot{M}_{\text{EDD}}\dot{m}, \quad (7)$$

where  $\dot{M}_{\text{crit}} = L_{\text{EDD}}/c^2$  is the critical accretion rate, and  $\dot{M}_{\text{EDD}} = L_{\text{EDD}}/(\eta c^2)$  is the Eddington accretion rate. Based on this equation,  $\dot{m}$  in Li & Cao (2008) is  $\eta$  ( $\sim 1/16$ ) times our  $\dot{m}$  as their  $\dot{m}$  is the ratio of  $\dot{M}$  to  $\dot{M}_{\text{EDD}}$ .

We calculate spectra for different black hole masses and accretion rates.  $M_{\text{BH}}$  equals to  $10^8$ ,  $10^{8.7}$  and  $10^9 M_{\odot}$  with an observational uncertainty of 0.4 dex (Vestergaard & Wilkes 2006), while  $R_{\text{EDD}}$  equals to 0.0316, 0.1259 and 0.3162 with an uncertainty of 0.3 dex (Kollmeier et al. 2006). After convolving with the SDSS filter response function, we convert the flux to the SDSS AB magnitude  $A(M_{\text{BH}}, \dot{m})$ . Assuming the change of  $\dot{m}$  is  $x\dot{m}$ , we adopt  $V = A(M_{\text{BH}}, \dot{m}) - A(M_{\text{BH}}, (1+x)\dot{m})$  as variability indicators. Results for the three  $x$  values (0.4, 0.2, 0.1) are shown as red, blue and black lines respectively in Fig. 20. At a specific  $x$ , the variability amplitudes along with their errors are calculated as below. A set of 100 normally-distributed random  $M_{\text{BH}}$  around  $10^{8.7} M_{\odot}$  and a set of 100 normally-distributed random  $R_{\text{EDD}}$  around 0.1259 are carried out within their observational uncertainties. Based on the set of  $M_{\text{BH}}$  and the set of  $R_{\text{EDD}}$ , we estimate variability amplitudes in each filter band to see its dependence on rest-frame wavelength. The mean value of the set of estimations and 3 times the standard deviation in each filter ( $u'$ ,  $g'$ ,  $r'$ ,  $i'$  and  $z'$ ) are adopted as the final variability and its uncertainty respectively, as shown in the upper left panel of Fig. 20. The variability amplitude declines with the increasing of rest-frame wavelength under the three changes of accretion rate. In the upper right panel, an anti-correlation between  $V$  in the  $r'$  band and  $R_{\text{EDD}}$  is displayed, where  $V$  and the error in  $V$  are respectively the mean value and 3 times the standard deviation of a set of variability amplitudes estimated from 100 random realizations of the model<sup>1</sup>. As luminosity is only related to  $R_{\text{EDD}}$  if  $M_{\text{BH}}$  is fixed, an inverse relation with  $L_{\text{bol}}$  is naturally expected. We do see this trend in the lower right panel of Fig. 20. For a set of 100 normally-distributed random  $R_{\text{EDD}}$  values around 0.1259 within its observational uncertainty, we obtained 3 sets of  $V$  values, each set with respect to one of the three  $M_{\text{BH}}$  values. The mean value and 3 times the dispersion of  $V$  values in each set is adopted as the final  $V$  and error in  $V$  for the  $M_{\text{BH}}$  value. As displayed in the lower left panel, there is an increase of optical variability with the increase of black hole mass. Comparisons between our theoretic results and observed relationships are carried out in each panel. We find that the variability amplitude caused by a change of accretion rate around  $0.2\dot{m}$  agrees well with the majority of variability amplitudes in observations. Moreover, besides the relation of variability with rest-frame wavelength, the model also reproduces the tendencies of correlations between the variability amplitude and luminosity, as well as accretion rate.

---

<sup>1</sup> $M_{\text{BH}}$  in the model is generated from a normal distribution with a mean value of  $10^{8.7} M_{\odot}$  and an observational uncertainty of 0.4 dex,  $\dot{m}$  is one of the three different  $\dot{m}$  and  $x\dot{m}$  refers to a change of the corresponding  $\dot{m}$ .

We fit the simulated data points as we do with the real data in the  $x = 0.2$  case, which are shown in the upper right of each panel. All the anti-correlations are flatter than the results from observations. The predicted correlation seems to be inconsistent with the weak anti-correlation between the variability amplitude and  $M_{\text{BH}}$  for the subsamples within small ranges of  $R_{\text{EDD}}$  as we stated in § 6. It suggests that other physical mechanisms may still need to be considered in modifying the simple accretion disk model.

## 8. Conclusion

A sample of 7658 quasars drawn from SDSS-DR7 is used to investigate the relationship between the variability amplitude and rest-frame wavelength, redshift and the intrinsic quasar parameters, i.e., black hole mass, bolometric luminosity and Eddington ratio. We analyzed the radio-quiet and radio-loud quasar variability properties with the sample. Because we have better quality data points for each quasar and a large sample, the variability indicator is calculated for each quasar from its long term light curve and the dependence of different parameters are disentangled by binning the parameter space into small slices. Our main conclusions are the following:

1. There is an anti-correlation between the variability amplitude and rest-frame wavelength after excluding the influences of redshift and the intrinsic parameters on variability amplitude. The quasar variability amplitude of radio-quiet quasars seems not dependent on redshift, while the possible anti-correlation between that of radio-loud quasars and redshift still needs be confirmed with a larger sample.

2. Although the median variability amplitude of the radio-loud quasars is similar compared to that of radio-quiet quasars, their intrinsic distributions are different. It implies that there may be some mechanisms other than the accretion disk instability behind the variability of radio-loud quasars.

3. There is a bluer-when-brighter color chromatism for both radio-quiet quasars and radio-loud ones. Some mechanisms, including instabilities occurring in the inner disk, the influence of the host galaxy, bright spots or a combination of them, may explain the chromatism.

4. The variability amplitude is significantly anti-correlated with  $R_{\text{EDD}}$  and  $L_{\text{bol}}$  in the subsamples without binning the quasar parameters. There is no certain correlation between the variability amplitude and  $M_{\text{BH}}$  in all these subsamples. After considering the relationships among the intrinsic quasar parameters, we find that small data sets still exhibit an anti-correlation between the variability amplitude and  $R_{\text{EDD}}$ , and between the variability

amplitude and  $L_{\text{bol}}$  with a lower significance level. Moreover, an anti-correlation of the variability amplitude with  $M_{\text{BH}}$  begins to emerge in bins of  $R_{\text{EDD}}$ , but a positive correlation with  $M_{\text{BH}}$  is shown in bins of  $L_{\text{bol}}$ .

5. Based on the Shakura-Sunyaev model, assuming the change of accretion rate as the origin of quasar variability, we reproduce the relationship of the variability amplitude with rest-frame wavelength with good agreement, and the tendencies of correlations between variability and  $R_{\text{EDD}}$  as well as  $L_{\text{bol}}$ . The predicted correlation between the variability amplitude and  $M_{\text{BH}}$  seems not to correspond well to the case inferred from observations, namely an anti-correlation with  $M_{\text{BH}}$  in small bins of  $R_{\text{EDD}}$ . It implies that the change of accretion rate is important for producing the observed optical variability but other physical mechanisms still need to be considered in modifying the simple accretion disk model for quasars.

We thank the anonymous referee for suggestion that have significantly improved the quality of this paper. We also thank Fukun Liu for helpful discussions on the relationship between variability and black hole mass. We acknowledge Tie Liu and Song Huang for helpful discussions on the statistical test of distributions of variability amplitudes. Thank Stephen Justham, Zhao-Yu Li and Awat Rahimi for reading the manuscript and providing various suggestions that have greatly improved the draft. This work was supported by an NSFC grant (No. 11033001) and the 973 program (No. 2007CB8154505) in China. Funding for the SDSS and SDSS-II has been provided by the Alfred P. Sloan Foundation, the Participating Institutions, the National Science Foundation, the U.S. Department of Energy, the National Aeronautics and Space Administration, the Japanese Monbukagakusho, the Max Planck Society, and the Higher Education Funding Council for England. The SDSS Web Site is <http://www.sdss.org/>. The SDSS is managed by the Astrophysical Research Consortium for the Participating Institutions. The Participating Institutions are the American Museum of Natural History, Astrophysical Institute Potsdam, University of Basel, University of Cambridge, Case Western Reserve University, University of Chicago, Drexel University, Fermilab, the Institute for Advanced Study, the Japan Participation Group, Johns Hopkins University, the Joint Institute for Nuclear Astrophysics, the Kavli Institute for Particle Astrophysics and Cosmology, the Korean Scientist Group, the Chinese Academy of Sciences (LAMOST), Los Alamos National Laboratory, the Max-Planck-Institute for Astronomy (MPIA), the Max-Planck-Institute for Astrophysics (MPA), New Mexico State University, Ohio State University, University of Pittsburgh, University of Portsmouth, Princeton University, the United States Naval Observatory, and the University of Washington.

## REFERENCES

- Ai, Y. L., Yuan, W., Zhou, H. Y., et al. 2010, *ApJ*, 716, L31
- Ai, Y. L., Yuan, W., Zhou, H. Y., Wang, T. G., & Zhang, S. H. 2011, *ApJ*, 727, 31
- Aretxaga, I., Cid Fernandes, R., & Terlevich, R. J. 1997, *MNRAS*, 286, 271
- Bauer, A., Baltay, C., Coppi, P., et al. 2009, *ApJ*, 696, 1241
- Becker, R. H., White, R. L., & Helfand, D. J. 1995, *ApJ*, 450, 559
- Bonoli, F., Braccisi, A., Federici, L., Zitelli, V., & Formiggini, L. 1979, *A&AS*, 35, 391
- Butler, N. R., & Bloom, J. S. 2011, *AJ*, 141, 93
- Cid Fernandes, R., Sodré, L., Jr., & Vieira da Silva, L., Jr. 2000, *ApJ*, 544, 123
- Courvoisier, T. J.-L., Paltani, S., & Walter, R. 1996, *A&A*, 308, L17
- Cristiani, S., Trentini, S., La Franca, F., et al. 1996, *A&A*, 306, 395
- Cristiani, S., Vio, R., & Andreani, P. 1990, *AJ*, 100, 56
- Cutri, R. M., Wisniewski, W. Z., Rieke, G. H., & Lebofsky, M. J. 1985, *ApJ*, 296, 423
- Czerny, B., Siemiginowska, A., Janiuk, A., & Gupta, A. C. 2008, *MNRAS*, 386, 1557
- di Clemente, A., Giallongo, E., Natali, G., Trevese, D., & Vagnetti, F. 1996, *ApJ*, 463, 466
- Frank, J., King, A., & Raine, D. J. 2002, *Accretion Power in Astrophysics*, by Juhan Frank and Andrew King and Derek Raine, pp. 398. ISBN 0521620538. Cambridge, UK: Cambridge University Press, February 2002.,
- Fukugita, M., Ichikawa, T., Gunn, J. E., et al. 1996, *AJ*, 111, 1748
- Giallongo, E., Trevese, D., & Vagnetti, F. 1991, *ApJ*, 377, 345
- Giveon, U., Maoz, D., Kaspi, S., Netzer, H., & Smith, P. S. 1999, *MNRAS*, 306, 637
- Hawkins, M. R. S. 1993, *Nature*, 366, 242
- Honma, F., Kato, S., & Matsumoto, R. 1991, *PASJ*, 43, 147
- Hook, I. M., McMahon, R. G., Boyle, B. J., & Irwin, M. J. 1994, *MNRAS*, 268, 305
- Ivezić, Ž., Smith, J. A., Miknaitis, G., et al. 2007, *AJ*, 134, 973

- Kato, S., Abramowicz, M. A., & Chen, X. 1996, PASJ, 48, 67
- Kawaguchi, T., Mineshige, S., Umemura, M., & Turner, E. L. 1998, ApJ, 504, 671
- Kollmeier, J. A., Onken, C. A., Kochanek, C. S., et al. 2006, ApJ, 648, 128
- Li, S.-L., & Cao, X. 2008, MNRAS, 387, L41
- MacLeod, C. L., Ivezić, Ž., Kochanek, C. S., et al. 2010, ApJ, 721, 1014
- Malkan, M. A. 1983, ApJ, 268, 582
- Manmoto, T., Takeuchi, M., Mineshige, S., Matsumoto, R., & Negoro, H. 1996, ApJ, 464, L135
- Meusinger, H., Hinze, A., & de, H. A. 2010, VizieR Online Data Catalog, 352, 59037
- Netzer, H., & Sheffer, Y. 1983, MNRAS, 203, 935
- Paltani, S., & Courvoisier, T. J.-L. 1997, A&A, 323, 717
- Paltani, S., & Courvoisier, T. J.-L. 1994, A&A, 291, 74
- Rees, M. J. 1984, ARA&A, 22, 471
- Sakata, Y., Morokuma, T., Minezaki, T., et al. 2011, ApJ, 731, 50
- Schmidt, K. B., Rix, H.-W., Jester, S., et al. 2010, IAU Symposium, 267, 265
- Schmidt, K. B., Rix, H.-W., Shields, J. C., et al. 2012, ApJ, 744, 147
- Schneider, D. P., Richards, G. T., Hall, P. B., et al. 2010, AJ, 139, 2360
- Sesar, B., Ivezić, Ž., Lupton, R. H., et al. 2007, AJ, 134, 2236
- Shakura, N. I., & Sunyaev, R. A. 1973, A&A, 24, 337
- Shen, Y., & Kelly, B. C. 2010, ApJ, 713, 41
- Shen, Y., Richards, G. T., Strauss, M. A., et al. 2011, ApJS, 194, 45
- Shields, G. A. 1978, Nature, 272, 706
- Terlevich, R., Tenorio-Tagle, G., Franco, J., & Melnick, J. 1992, MNRAS, 255, 713
- Torricelli-Ciamponi, G., Foellmi, C., Courvoisier, T. J.-L., & Paltani, S. 2000, A&A, 358, 57

- Trèvese, D., & Vagnetti, F. 2002, *ApJ*, 564, 624
- Trèvese, D., & Vagnetti, F. 2001, *Mem. Soc. Astron. Italiana*, 72, 33
- Trevese, D., Kron, R. G., Majewski, S. R., Bershad, M. A., & Koo, D. C. 1994, *ApJ*, 433, 494
- Vanden Berk, D. E., Wilhite, B. C., Kron, R. G., et al. 2004, *ApJ*, 601, 692
- Vestergaard, M., & Wilkes, B. J. 2001, *ApJS*, 134, 1
- White, R. L., Becker, R. H., Helfand, D. J., & Gregg, M. D. 1997, *VizieR Online Data Catalog*, 8048, 0
- Wilhite, B. C., Brunner, R. J., Grier, C. J., Schneider, D. P., & vanden Berk, D. E. 2008, *MNRAS*, 383, 1232
- Wilhite, B. C., Vanden Berk, D. E., Kron, R. G., et al. 2005, *ApJ*, 633, 638
- Wold, M., Brotherton, M. S., & Shang, Z. 2007, *MNRAS*, 375, 989



Table 1. The bin details of each parameter

Parameter	Minimum	Maximum	Bin size	$N_{\text{bins}}$
(1)	(2)	(3)	(4)	(4)
$z$	0.08	4.9	0.3	16
$\log M_{\text{BH}} (M_{\odot})$	7.5	10.5	0.5	6
$\log L_{\text{bol}} (\text{erg/s})$	44.5	48	0.5	7
$\log R_{\text{EDD}}$	-2.0	0.5	0.5	5

Note. — Col. (1) Parameter names. Col. (2) Minimum value of the binned parameter in Col. (1). Col. (3) Maximum value of the binned parameter in Col. (1). Col. (4) Bin interval of the binned parameter in Col. (1). Note the first bin size of  $z$  is 0.32. Col. (5) Number of bins.

Table 2. Correlation between variability and each parameter

Radio loudness	Parameter	Restricted Parameters			Spearman relation		Pearson relation	Linear fit	
		$x1$	$x2$	$x3$	$r1$	$p$	$r2$	$b$	$a$
(1)	(2)	(3)	(4)	(5)	(6)	(7)	(8)	(9)	(10)
radio-quiet	$\log \lambda_{\text{rf}}$	$R_{\text{EDD}}$	$z$	$M_{\text{BH}}$	-0.229	0.019	-0.233	$-0.137 \pm 0.052$	$0.579 \pm 0.180$
radio-quiet	$\log z$	$R_{\text{EDD}}$	$M_{\text{BH}}$	$\lambda_{\text{rf}}$	-0.081	0.189	-0.090	$-0.049 \pm 0.044$	$0.131 \pm 0.009$
radio-quiet	$\log L_{\text{bol}}$	$z$	$R_{\text{EDD}}$	$\lambda_{\text{rf}}$	-0.269	0.015	-0.260	$-0.044 \pm 0.020$	$2.128 \pm 0.913$
radio-quiet	$\log L_{\text{bol}}$	$z$	$M_{\text{BH}}$	$\lambda_{\text{rf}}$	-0.343	0.003	-0.335	$-0.063 \pm 0.020$	$3.032 \pm 0.926$
radio-quiet	$\log R_{\text{EDD}}$	$z$	$L_{\text{bol}}$	$\lambda_{\text{rf}}$	-0.167	0.137	-0.147	$-0.020 \pm 0.014$	$0.091 \pm 0.011$
radio-quiet	$\log R_{\text{EDD}}$	$z$	$M_{\text{BH}}$	$\lambda_{\text{rf}}$	-0.303	0.013	-0.299	$-0.052 \pm 0.019$	$0.075 \pm 0.013$
radio-quiet	$\log M_{\text{BH}}$	$z$	$L_{\text{bol}}$	$\lambda_{\text{rf}}$	0.113	0.235	0.104	$0.013 \pm 0.014$	$-0.002 \pm 0.119$
radio-quiet	$\log M_{\text{BH}}$	$z$	$R_{\text{EDD}}$	$\lambda_{\text{rf}}$	-0.203	0.057	-0.201	$-0.033 \pm 0.019$	$0.394 \pm 0.168$
radio-loud	$\log \lambda_{\text{rf}}$	$R_{\text{EDD}}$	$z$	$M_{\text{BH}}$	-0.187	0.218	-0.224	$-0.225 \pm 0.143$	$0.950 \pm 0.494$
radio-loud	$\log z$	$R_{\text{EDD}}$	$M_{\text{BH}}$	$\lambda_{\text{rf}}$	-0.153	0.306	-0.062	$-0.034 \pm 0.116$	$0.148 \pm 0.028$
radio-loud	$\log L_{\text{bol}}$	$z$	$R_{\text{EDD}}$	$\lambda_{\text{rf}}$	-0.266	0.297	-0.269	$-0.058 \pm 0.054$	$2.794 \pm 2.456$
radio-loud	$\log L_{\text{bol}}$	$z$	$M_{\text{BH}}$	$\lambda_{\text{rf}}$	-0.384	0.164	-0.321	$-0.071 \pm 0.055$	$3.373 \pm 2.536$
radio-loud	$\log R_{\text{EDD}}$	$z$	$L_{\text{bol}}$	$\lambda_{\text{rf}}$	-0.304	0.300	-0.274	$-0.045 \pm 0.032$	$0.079 \pm 0.035$
radio-loud	$\log R_{\text{EDD}}$	$z$	$M_{\text{BH}}$	$\lambda_{\text{rf}}$	-0.369	0.188	-0.291	$-0.069 \pm 0.047$	$0.056 \pm 0.055$
radio-loud	$\log M_{\text{BH}}$	$z$	$L_{\text{bol}}$	$\lambda_{\text{rf}}$	0.246	0.386	0.212	$0.040 \pm 0.035$	$-0.206 \pm 0.309$
radio-loud	$\log M_{\text{BH}}$	$z$	$R_{\text{EDD}}$	$\lambda_{\text{rf}}$	-0.220	0.432	-0.180	$-0.052 \pm 0.052$	$0.600 \pm 0.477$

Note. — Col. (1) The samples, namely the radio-quiet (radio-loud) subsample contains quasars with radio loudness smaller (larger) than 10. Col. (2) The parameter on which the dependence of variability is to be considered. Cols. (3-5) Parameters which are restricted in small ranges to exclude their influences on variability, denoted by  $x1$ ,  $x2$  and  $x3$ . Cols. (6-7)  $r1$  is the median value of Spearman rank correlation coefficients in all the qualified small data sets, which are obtained from binning in the restricted parameters, while  $p$  is the median value of the significance of its deviation from 0. Col. (8)  $r2$  is the median value of Pearson Product Correlation Coefficient, indicating the strength of linear correlations. Cols. (9-10)  $b$  is the median slope of the linear fitting for the dependence of the variability amplitude on the parameter denoted in Col.(2) and  $a$  is the median y axis intercept of the linear fit.

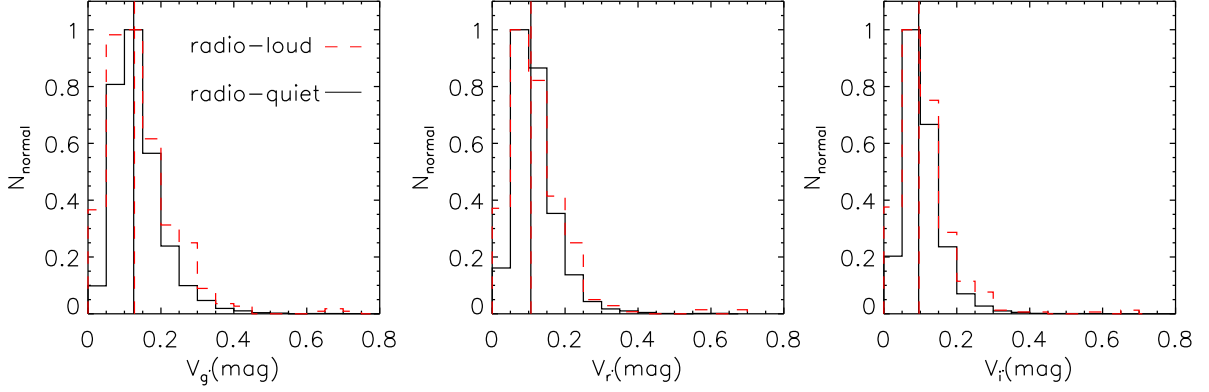


Fig. 1.— Normalized distribution of the variability amplitudes in the  $g'$ ,  $r'$  and  $i'$  band for the 416 radio-loud sources (red dashed lines) and 7242 radio-quiet sources (black solid lines). The median values are shown with the vertical lines.

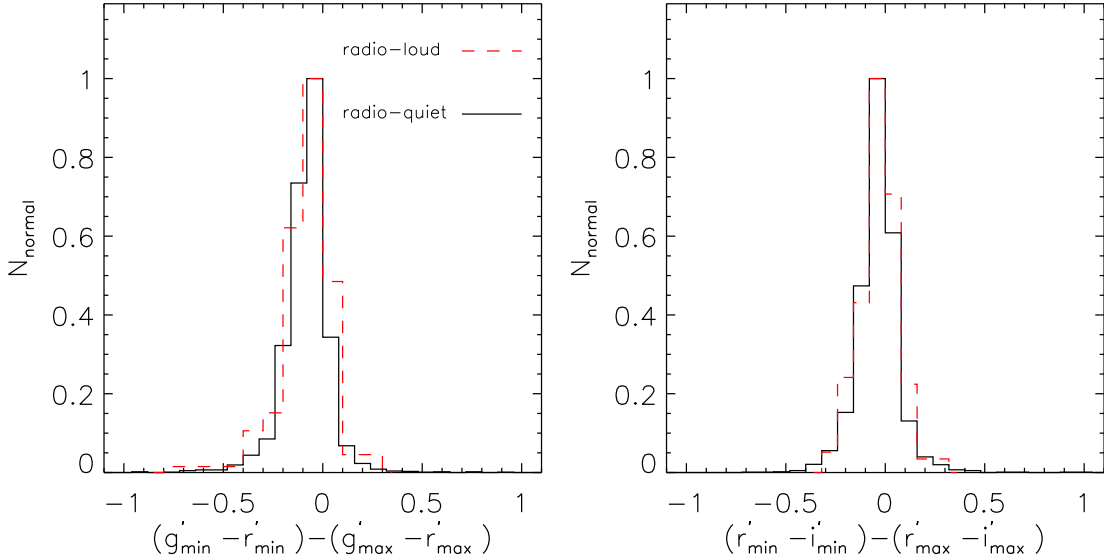


Fig. 2.— Normalized distributions of the color differences between the brightest state and faintest state. There are 166 radio-loud (red dashed lines) and 2811 radio-quiet quasars (black solid lines) in the left panel, 158 radio-loud and 2553 radio-quiet quasars in the right panel, respectively.

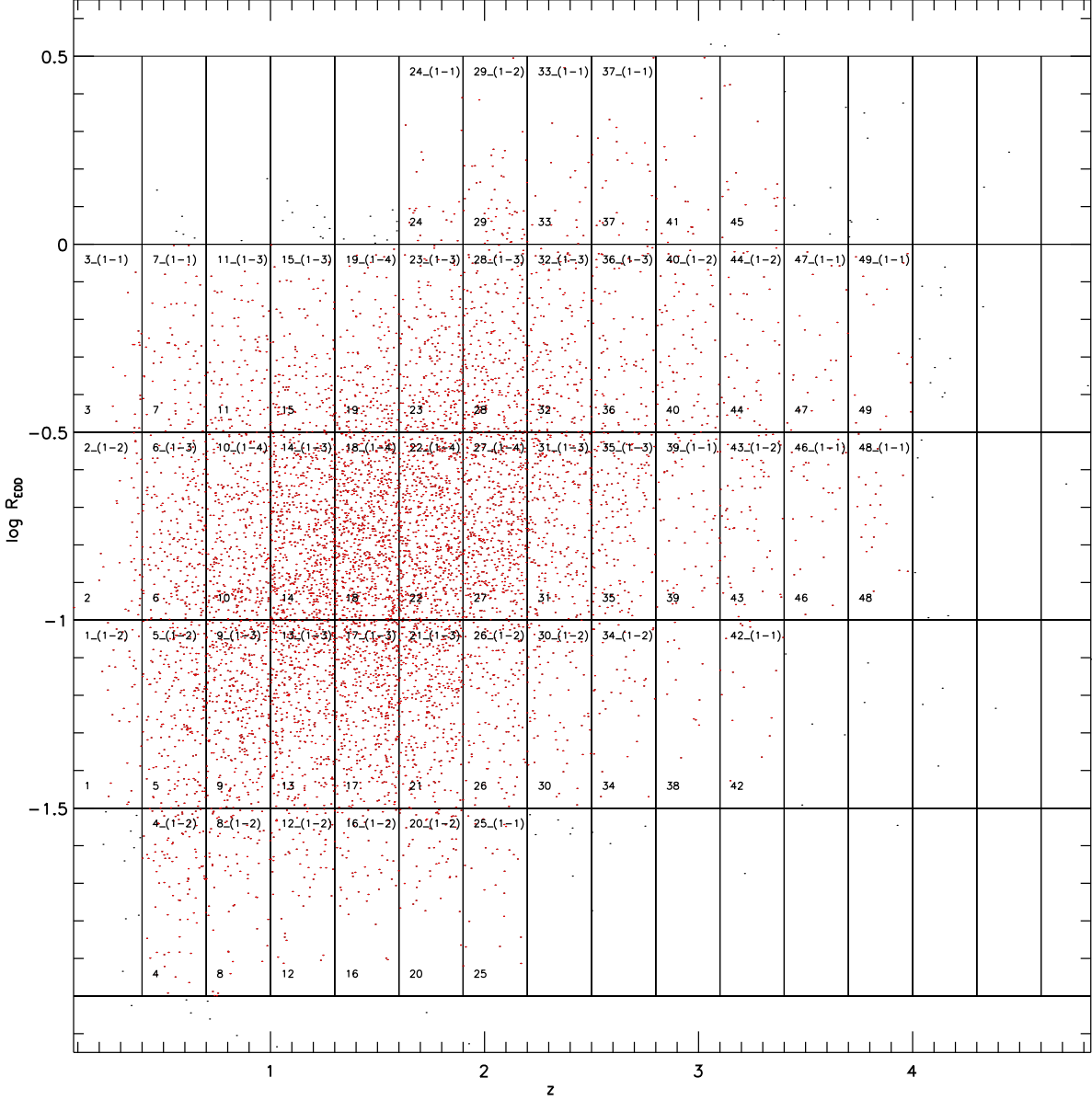


Fig. 3.—  $\log R_{\text{EDD}}$  vs.  $z$  for the 7242 radio-quiet quasars. The bin size of  $R_{\text{EDD}}$  and  $z$  are 0.5 dex and 0.3 respectively. Lines over-plotted divide quasars into  $16 \times 5$  subsamples. The 49 grids filled with red points refer to the qualified subsamples and they are marked with algebraic numbers in the lower corner of each grid. They are further separated into sub-subsamples with  $\log M_{\text{BH}}$  bin size of 0.5 dex. The algebraic numbers in the upper corner of the grids represent the indices of qualified sub-subsamples (with more than 10 quasars in each) for the study of the dependence of the variability amplitude on  $\lambda_{\text{rf}}$ .

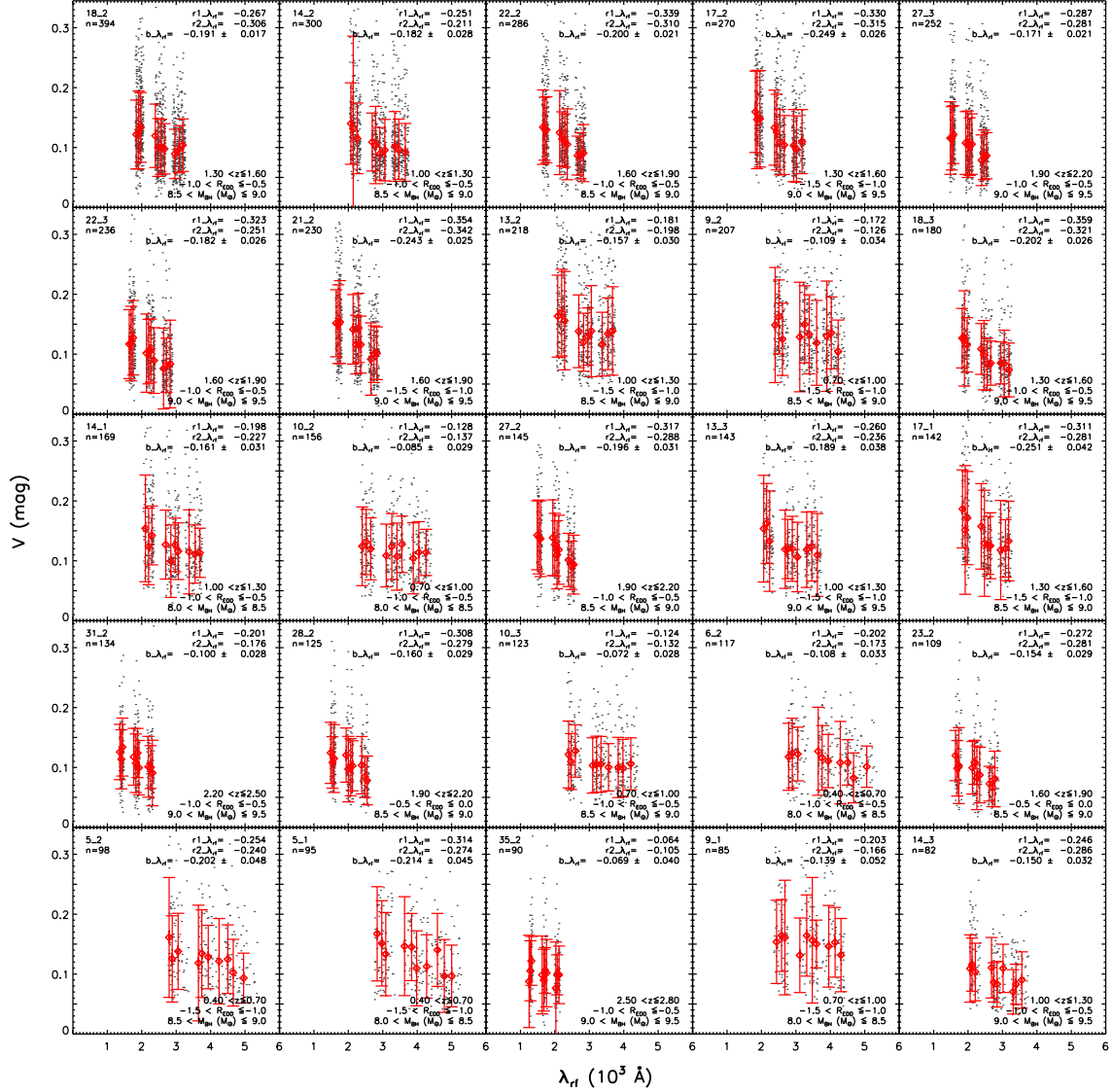


Fig. 4.— Dependence of  $V$  on  $\lambda_{rf}$  in the  $g'$ ,  $r'$  and  $i'$  band. To demonstrate the relation, only that for the 25 largest qualified sub-samples obtained from Fig. 3 are shown. In each panel, the 10 red diamonds refer to the median values of  $V$  and  $\lambda_{rf}$  in the bins obtained from evenly dividing  $\lambda_{rf}$  of the sub-sample. The legends in the upper left corner of each panel show the index of the sub-sample obtained from Fig. 3 and the number of quasars it contains.  $r1_{\lambda_{rf}}$ ,  $r2_{\lambda_{rf}}$  and  $b_{\lambda_{rf}}$  are displayed in the upper right corner and ranges of restricted parameters are shown in the lower right corner. For the radio-loud quasars, refer to Fig. 21 in the Appendix.

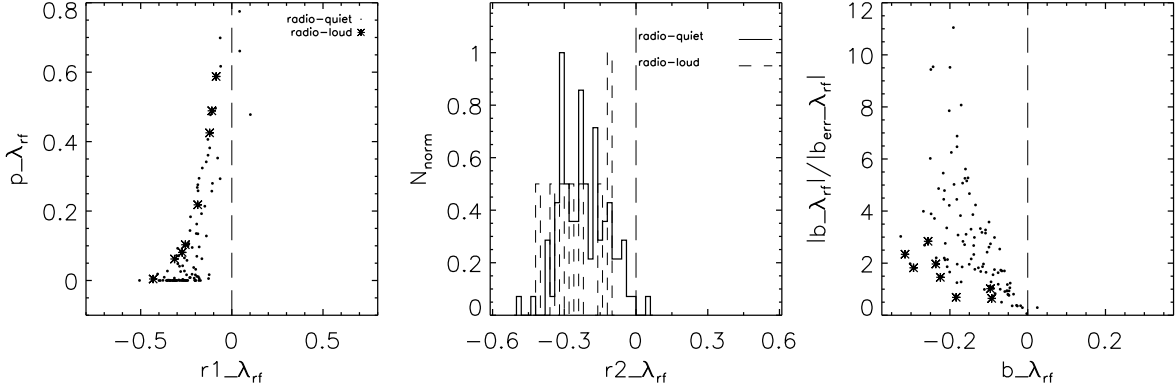


Fig. 5.— Statistical results for the relationships between  $V$  and  $\log \lambda_{\text{rf}}$ :  $p_{-\lambda_{\text{rf}}}$  vs  $r1_{-\lambda_{\text{rf}}}$  (left panel),  $r2_{-\lambda_{\text{rf}}}$  (middle panel) and the linear fit results,  $|b_{-\lambda_{\text{rf}}}|/|b_{\text{err}-\lambda_{\text{rf}}}|$  vs  $b_{-\lambda_{\text{rf}}}$  (right panel). Dots and solid lines refer to results of the radio-quiet subsamples, while asterisk signs and dashed lines refer to results of the radio-loud ones.

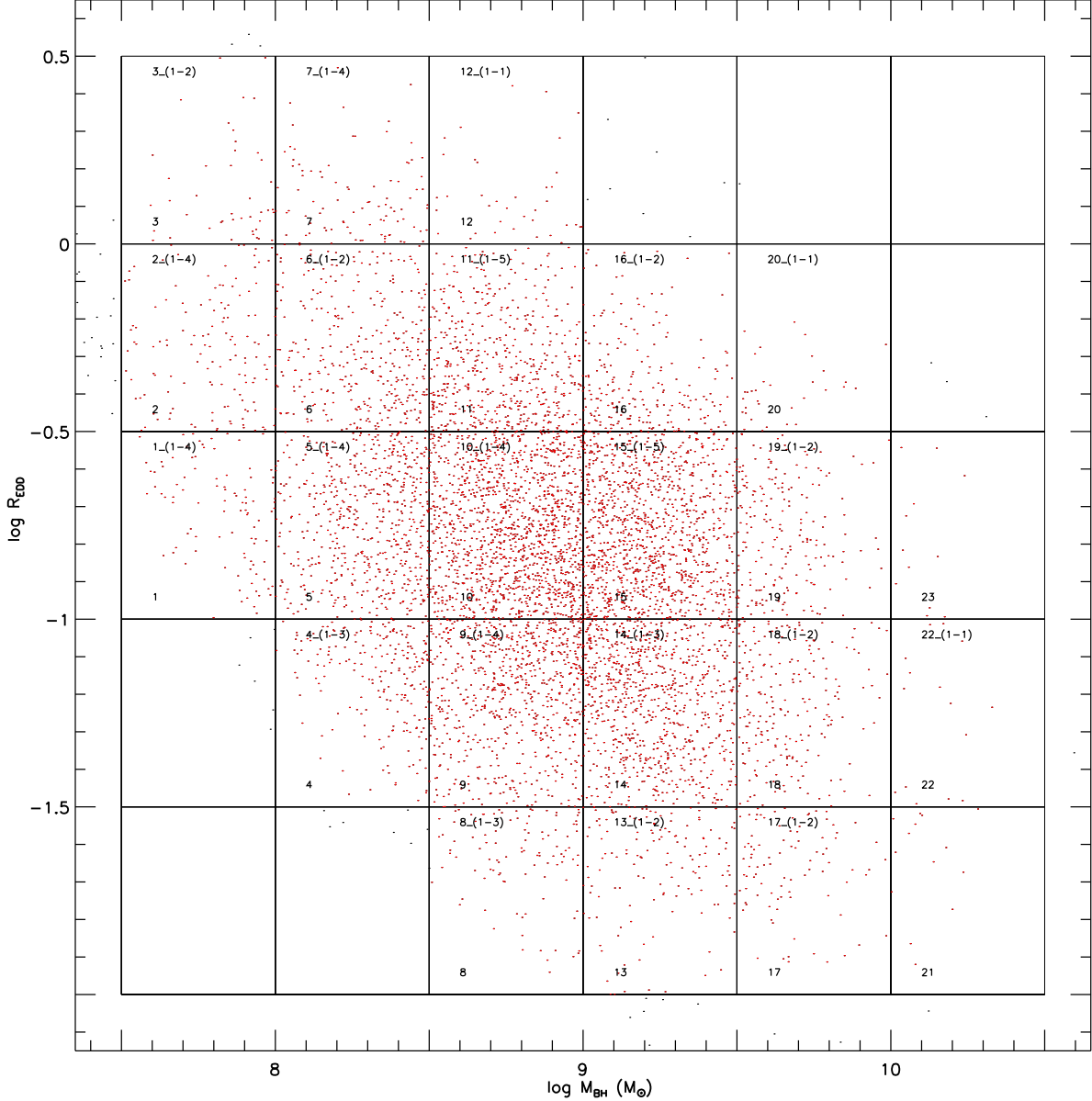


Fig. 6.—  $\log R_{\text{EDD}}$  vs.  $\log M_{\text{BH}}$  for the 7242 radio-quiet quasars. Their bin size are both 0.5 dex. Among  $5 \times 6$  subsamples divided by the overdrawn lines, 23 subsamples with more than 10 quasars in each (marked with algebraic numbers in the lower corner of each grid) are further divided into sub-subsamples with the  $\lambda_{\text{rf}}$  bin size of  $400 \text{ \AA}$  (see § 5 for more details). The algebraic numbers in the upper corner of the grids refer to the indices of the qualified sub-subsamples for the study of the dependence of  $V$  on  $z$ .

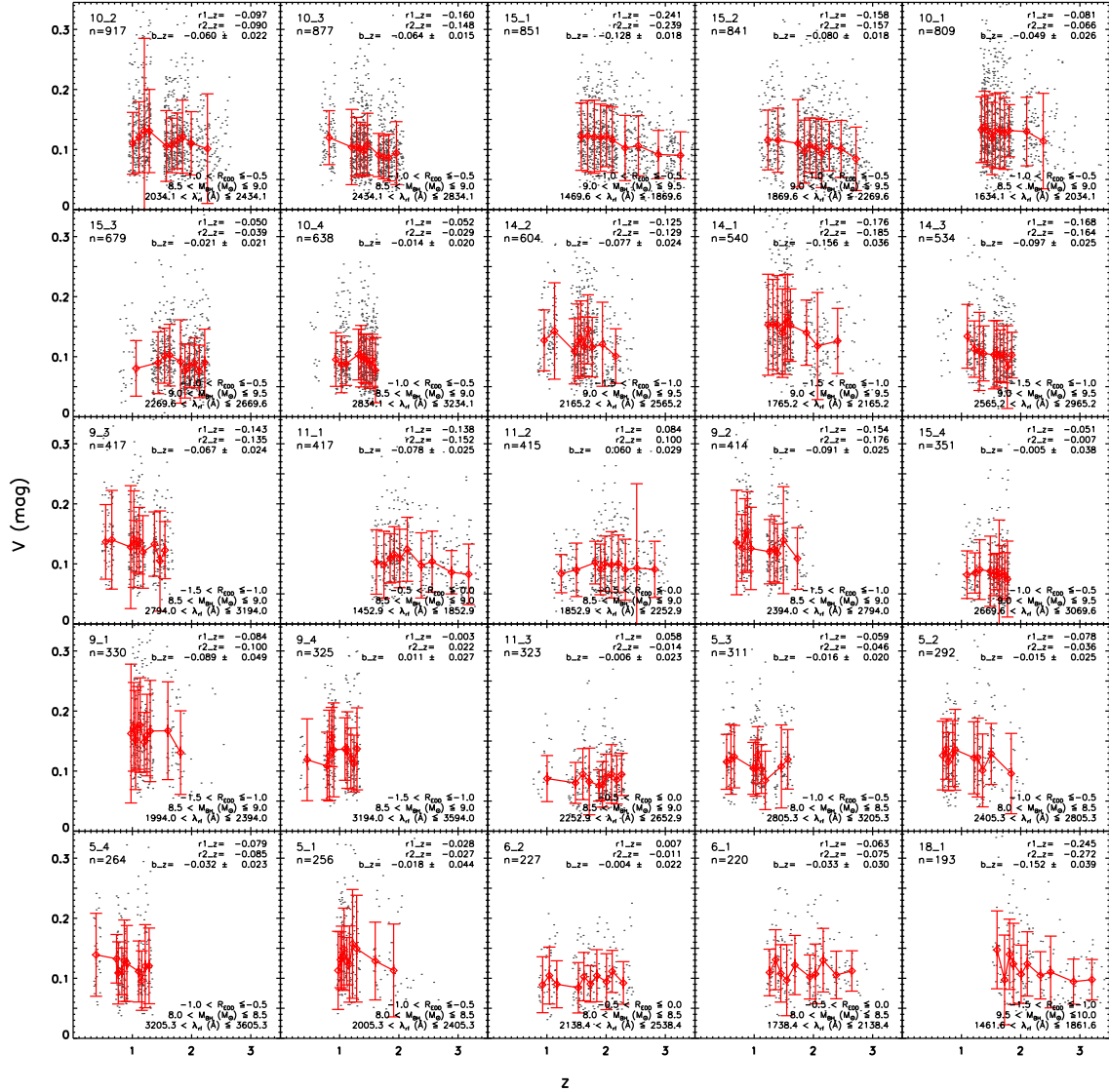


Fig. 7.— Dependence of  $V$  on  $z$  in the  $g'$ ,  $r'$  and  $i'$  band for the 25 largest qualified subsamples extracted from Fig. 6. In each panel, the 10 diamonds refer to the median values of  $V$  and  $z$  in bins from evenly dividing  $z$ . The texts in each panel have the same meaning with Fig. 4. For the radio-loud quasars, refer to Fig. 22 in the Appendix.



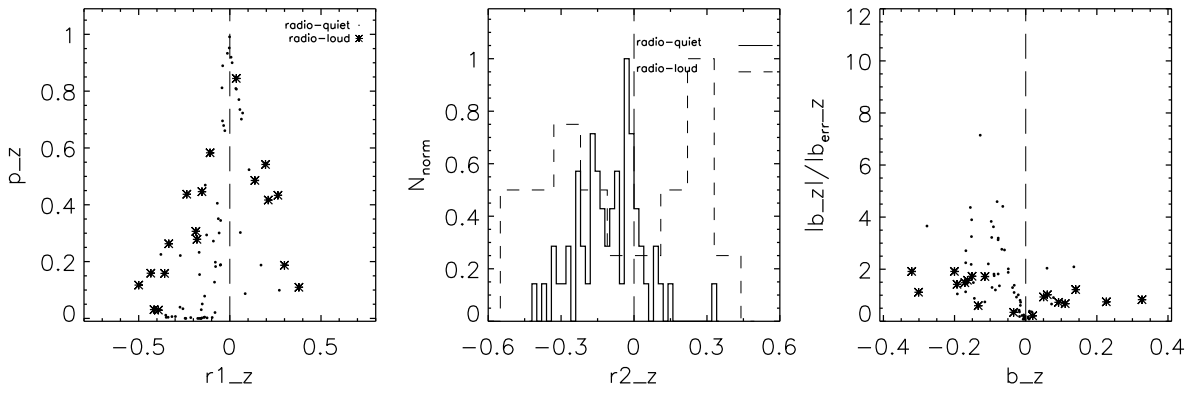


Fig. 8.— Figure similar to Fig. 5, but for the statistical results of the relationship between  $V$  and  $\log z$ .

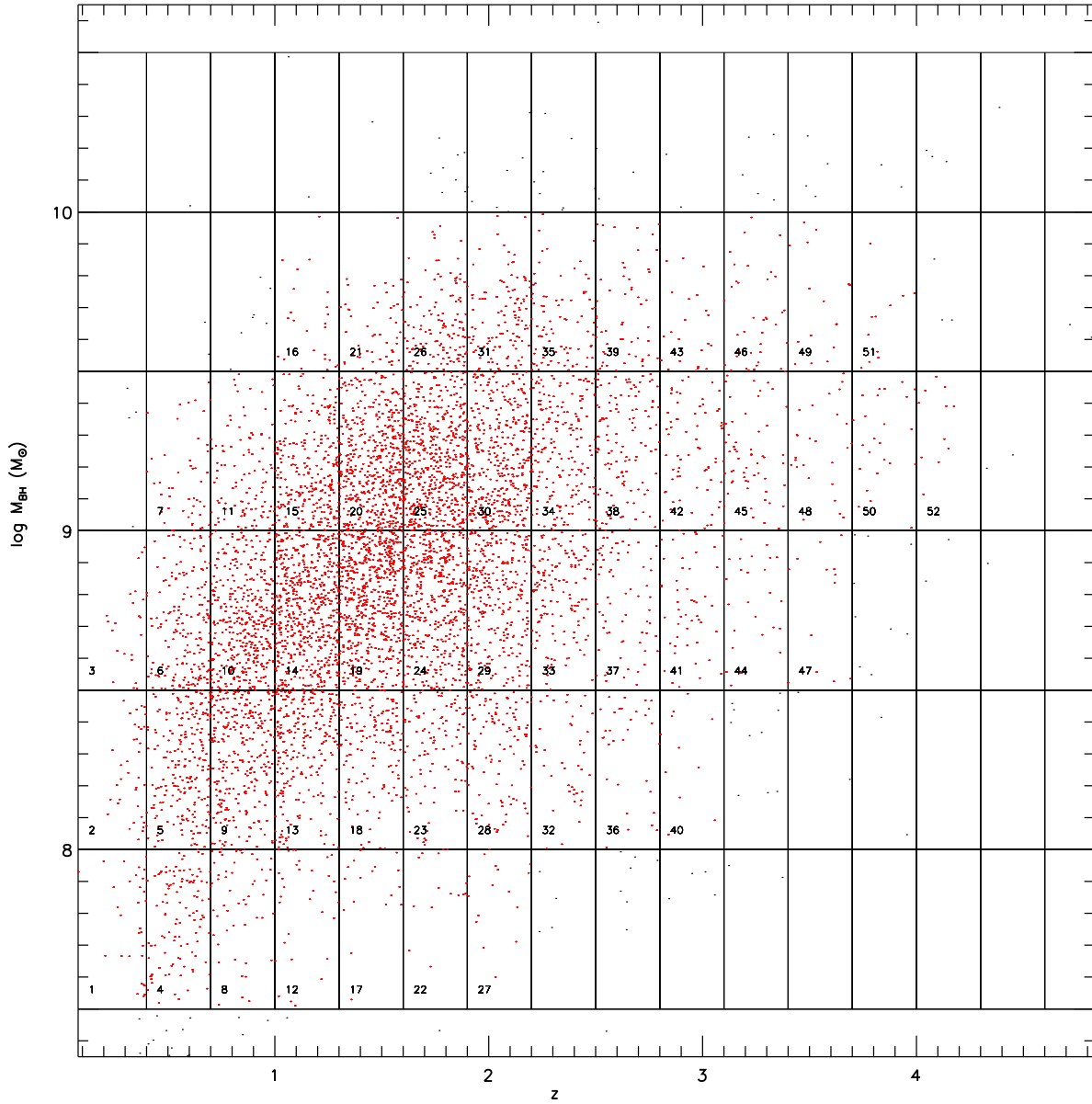


Fig. 9.—  $\log M_{\text{BH}}$  vs.  $z$  for the 7242 radio-quiet quasars. Their bin sizes are 0.5 dex and 0.3 respectively. Among  $6 \times 16$  subsamples divided by overdrawn lines, 52 subsamples with more than 10 quasars in each are qualified, represented by the grids filled with red points and marked with algebraic numbers.

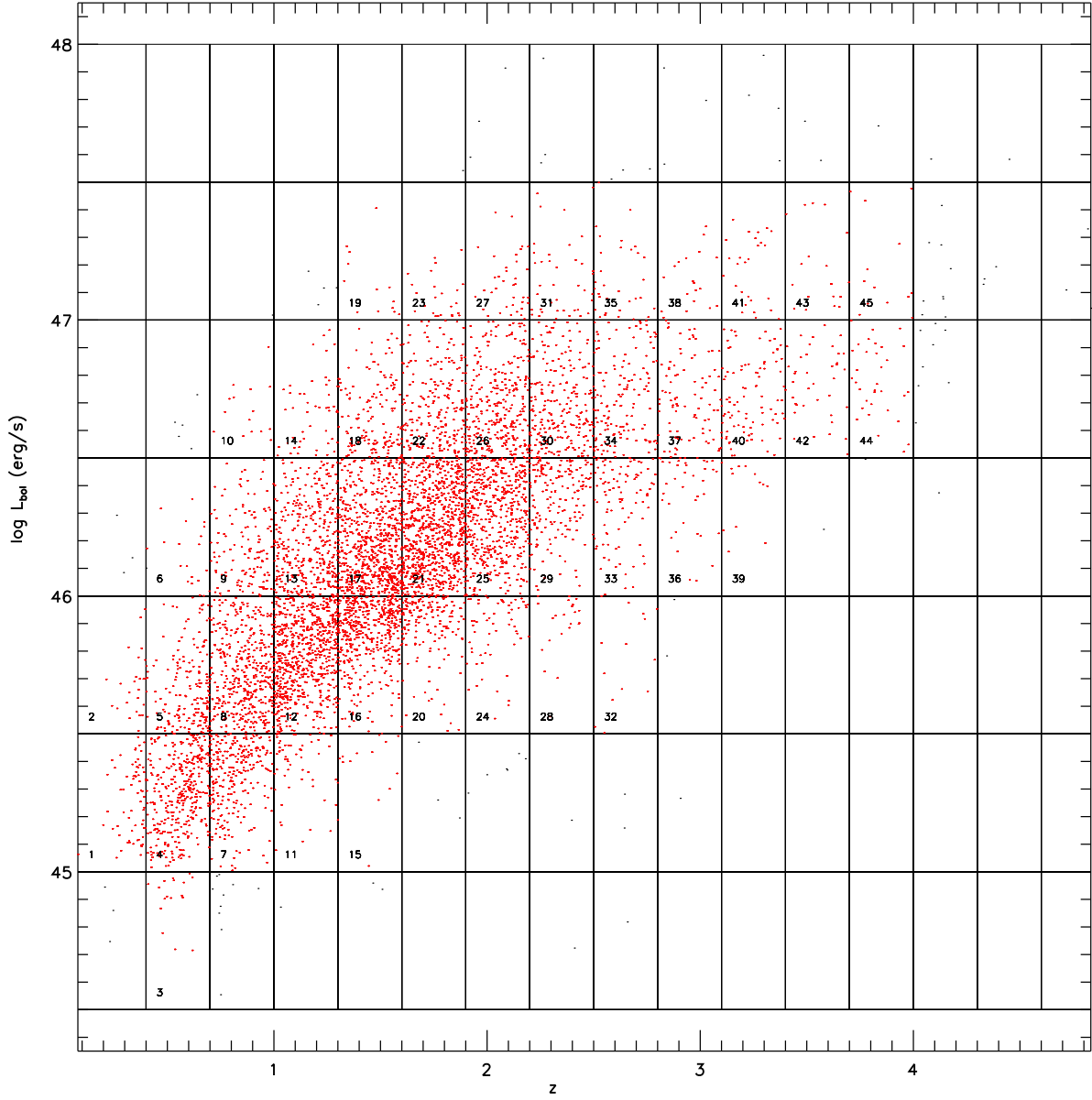


Fig. 10.—  $\log L_{\text{bol}}$  vs.  $z$  for the 7242 radio-quiet quasars. Their bin sizes are 0.5 dex and 0.3 respectively. Among  $7 \times 16$  subsamples divided by overdrawn lines, 45 subsamples with more than 10 quasars in each are qualified, represented by the grids filled with red points and marked with algebraic numbers.

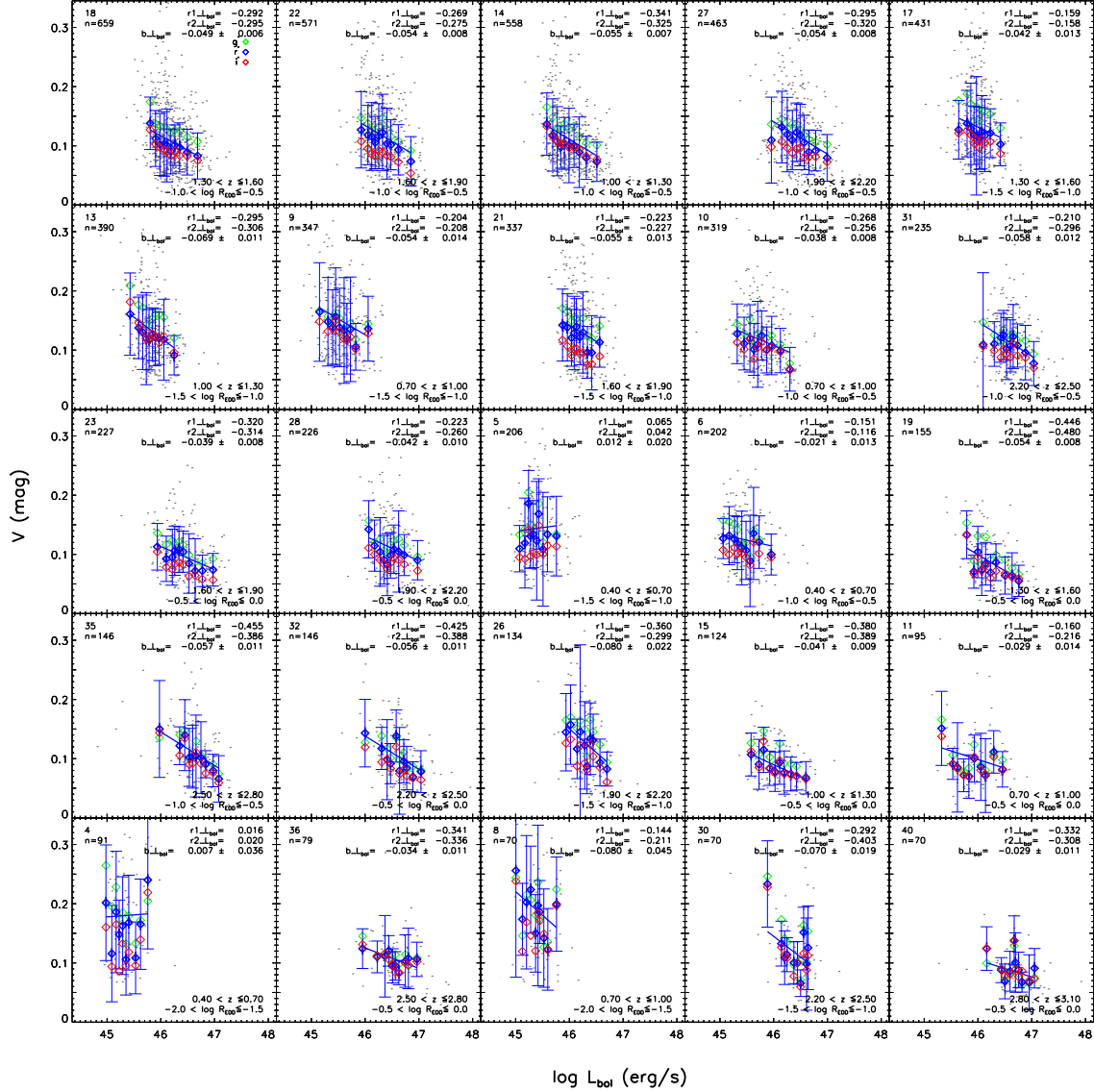


Fig. 11.— Dependence of  $V$  in the  $g'$ ,  $r'$  and  $i'$  filter band on  $L_{\text{bol}}$  for the 25 largest qualified subsamples obtained from the  $\log R_{\text{EDD}}-z$  space as shown in Fig. 3. In each panel, only  $V$  in the  $r'$  band for all the quasars are represented by grey points. The  $10 \times 3$  colored diamonds (green, blue and red) show the median  $V$  values in the 3 bands ( $g'$ ,  $r'$  and  $i'$ ) in the bins obtained from evenly dividing  $\log L_{\text{bol}}$ . The blue lines represent the linear fits for all the data in the  $r'$  band. The legends in the upper right corner of each panel list the  $r1-L_{\text{bol}}$ ,  $r2-L_{\text{bol}}$  and  $b-L_{\text{bol}}$  for the study of the variability amplitudes in the  $r'$  band, while the texts in the lower right corner of each panel give the ranges of restricted parameters. For the radio-loud quasars, refer to Fig. 23 in the Appendix.

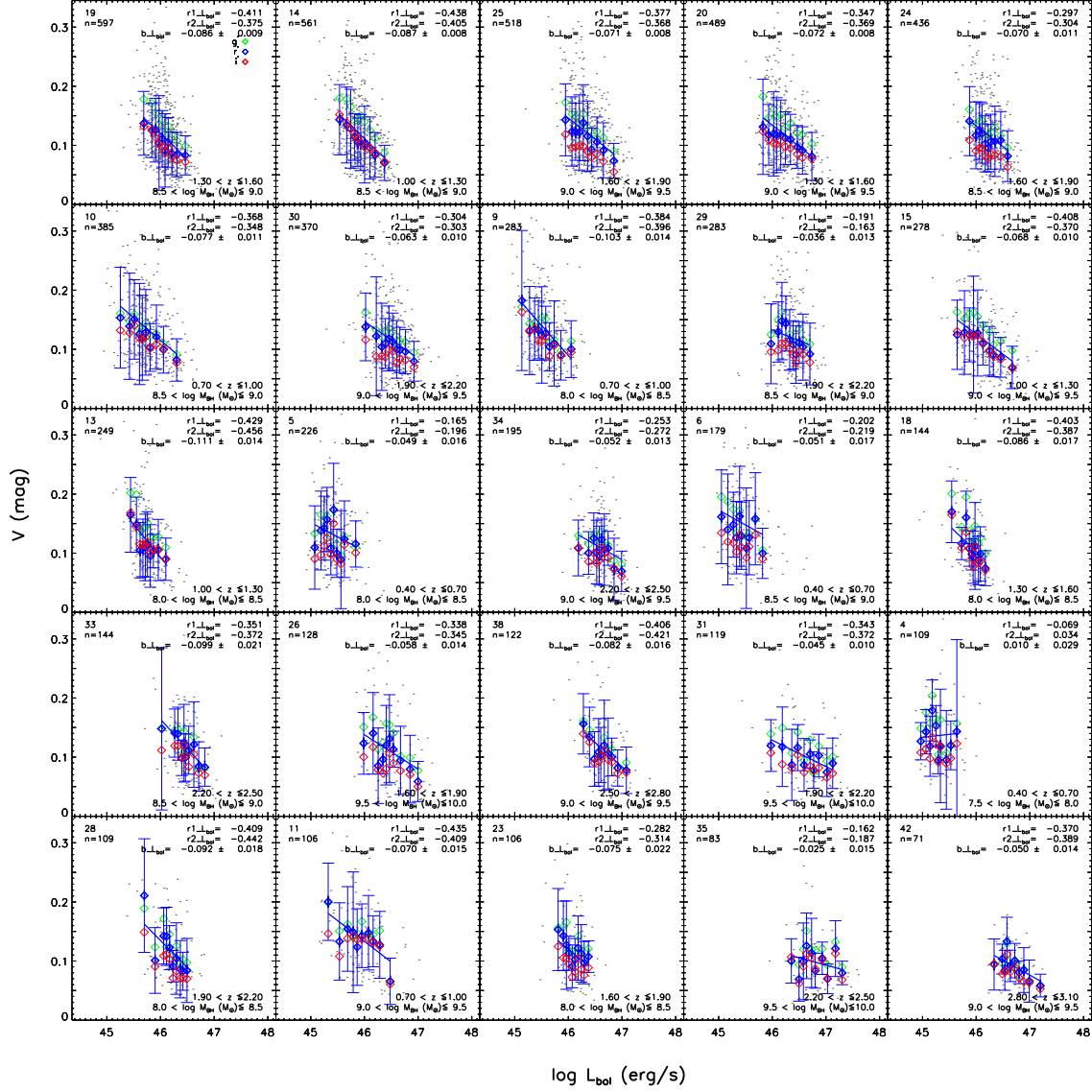


Fig. 12.— Figure similar to Fig. 11, but for the 25 largest qualified subsamples obtained from the  $\log M_{\text{BH}}-z$  space as displayed in Fig. 9. Refer to Fig. 24 in the Appendix with respect to the radio-loud quasars.

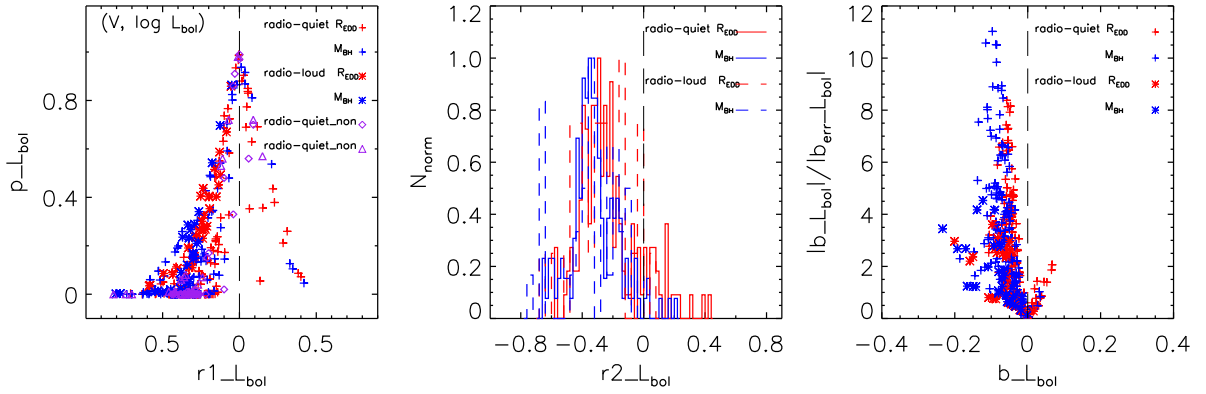


Fig. 13.— Figure similar to Fig. 5, but for the statistical results of the relationship between  $V$  and  $\log L_{bol}$ . The magenta diamonds and triangles show respectively the results of the radio-quiet and radio-loud subsamples. These subsamples are only binned in redshift, thus without excluding the relations among the three intrinsic quasar parameters. The blue signs and lines represent results of the subsamples obtained from the  $\log M_{BH}-z$  space and red ones refer to results of the subsamples binned in the  $\log R_{EDD}-z$  space.

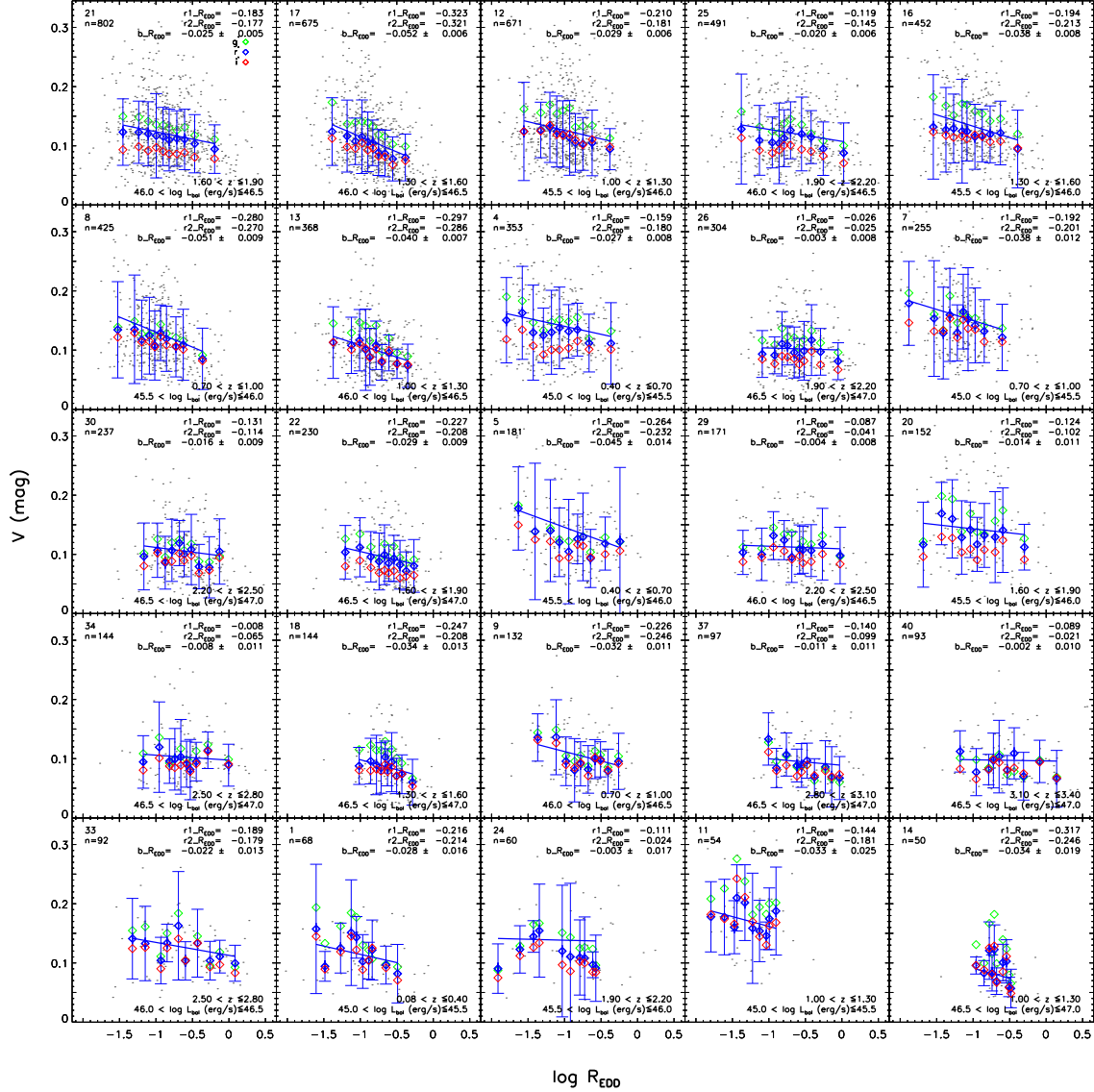


Fig. 14.— Dependence of  $V$  in the  $g'$ ,  $r'$  and  $i'$  filter band on  $R_{\text{EDD}}$  for the 25 largest qualified subsamples obtained from the  $\log L_{\text{bol}}-z$  space as shown in Fig. 10. In each panel, only  $V$  in the  $r'$  band for all the quasars are represented by grey points. The  $10 \times 3$  colored diamonds (green, blue and red) show the median  $V$  values in the 3 bands ( $g'$ ,  $r'$  and  $i'$ ) in the bins obtained from evenly dividing  $\log R_{\text{EDD}}$ . The blue lines represent the linear fits for all the data in the  $r'$  band. The legends in the upper right corner of each panel list the  $r1_{R_{\text{EDD}}}$ ,  $r2_{R_{\text{EDD}}}$  and  $b_{R_{\text{EDD}}}$  for the study of the variability amplitudes in the  $r'$  band, while the texts in the lower right corner of each panel show the ranges of the restricted parameters. Refer to Fig. 25 in the Appendix for the radio-loud quasars.



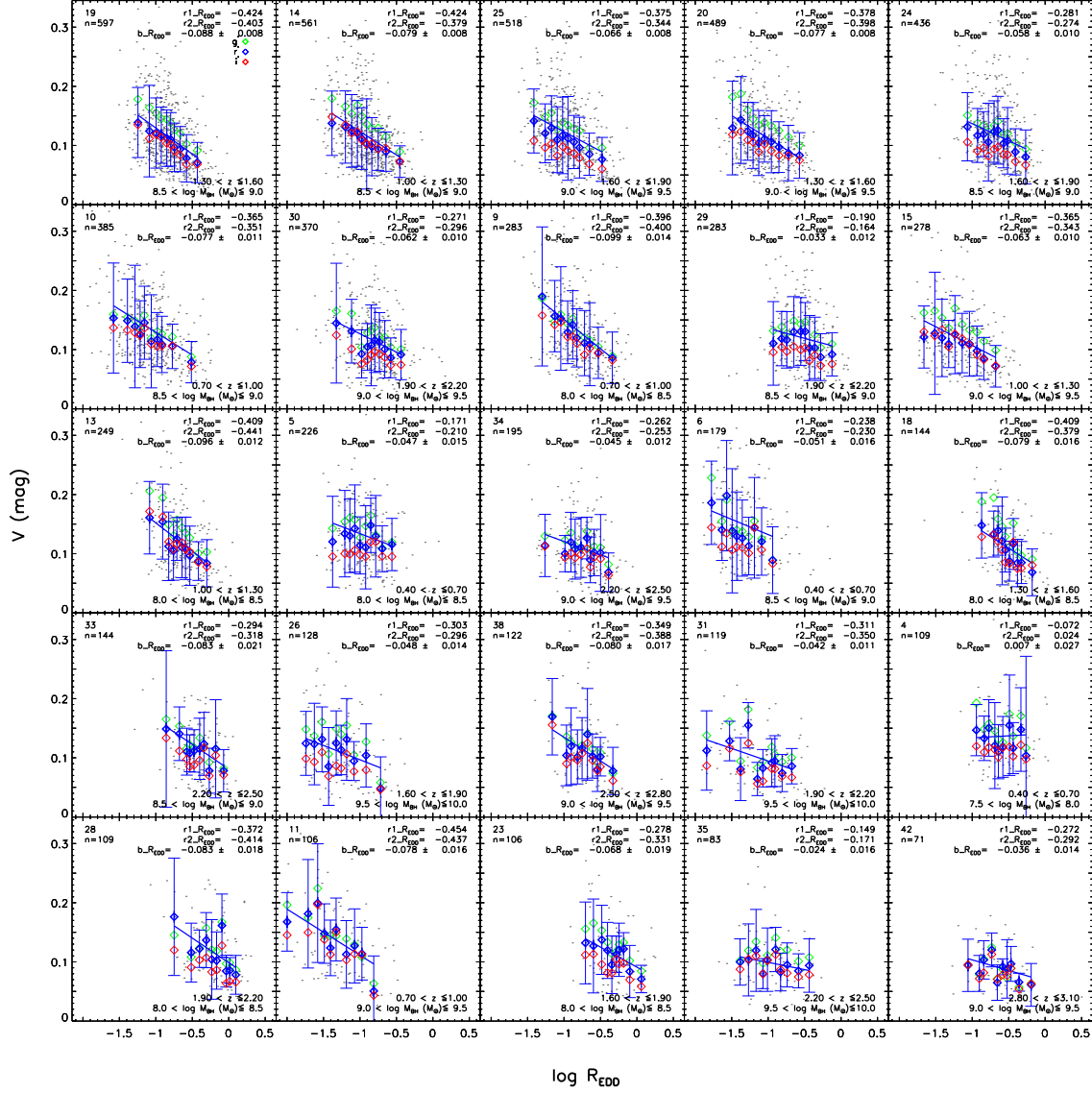


Fig. 15.— Figure similar to Fig. 14, but for the 25 largest qualified subsamples obtained from the  $\log M_{\text{BH}}-z$  space as shown in Fig. 9. Refer to Fig. 26 in the Appendix for the radio-loud quasars.

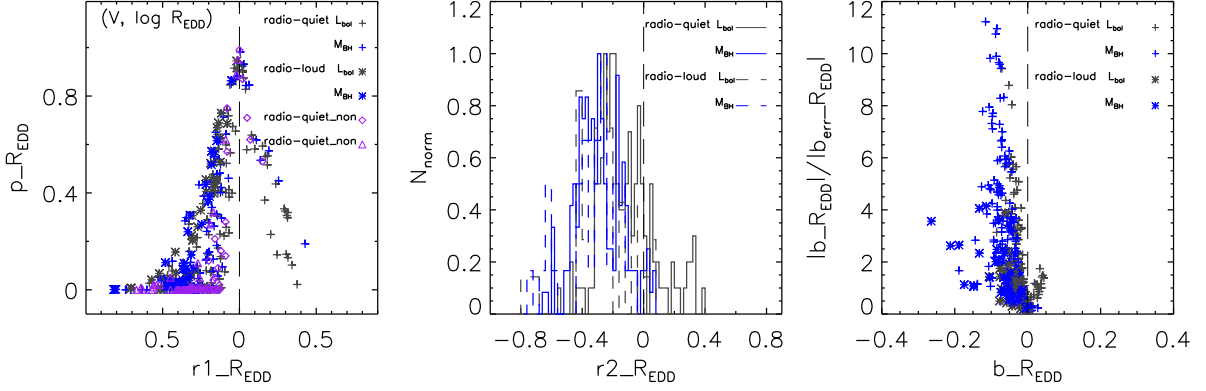


Fig. 16.— Figure similar to Fig. 13, but for the statistical results of the relationships between  $V$  and  $\log R_{\text{EDD}}$ . The grey signs and lines represent results of the subsamples obtained from the  $\log L_{\text{bol}}-z$  space and blue ones represent results of the subsamples obtained from the  $\log M_{\text{BH}}-z$  space.

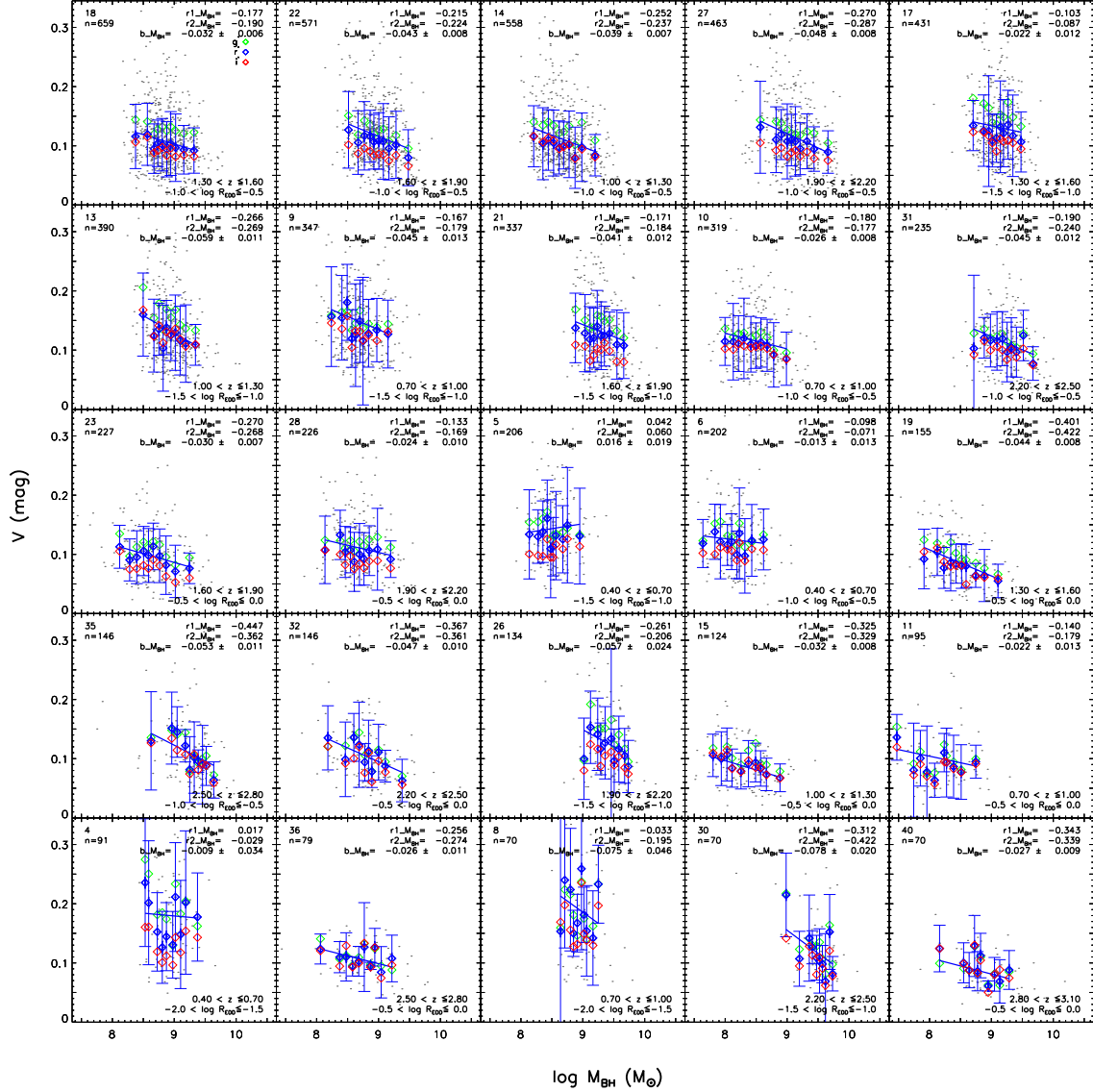


Fig. 17.— Dependence of  $V$  in the  $g'$ ,  $r'$  and  $i'$  filter band on  $M_{\text{BH}}$  for the 25 largest qualified subsamples obtained from the  $\log R_{\text{EDD}}-z$  space as shown in Fig. 3. In each panel, only  $V$  in the  $r'$  band for all the quasars are represented by grey points. The  $10 \times 3$  colored diamonds (green, blue and red) show the median  $V$  values in the 3 bands ( $g'$ ,  $r'$  and  $i'$ ) in the bins obtained from evenly dividing  $\log M_{\text{BH}}$ . The blue lines represent the linear fits for all the data in the  $r'$  band. The legends in the upper right corner of each panel list the  $r1_{M_{\text{BH}}}$ ,  $r2_{M_{\text{BH}}}$  and  $b_{M_{\text{BH}}}$  for the study of the variability amplitudes in the  $r'$  band, while the texts in the lower right corner of each panel give the ranges of the restricted parameters. For the radio-loud quasars refer to Fig. 27 in the Appendix.

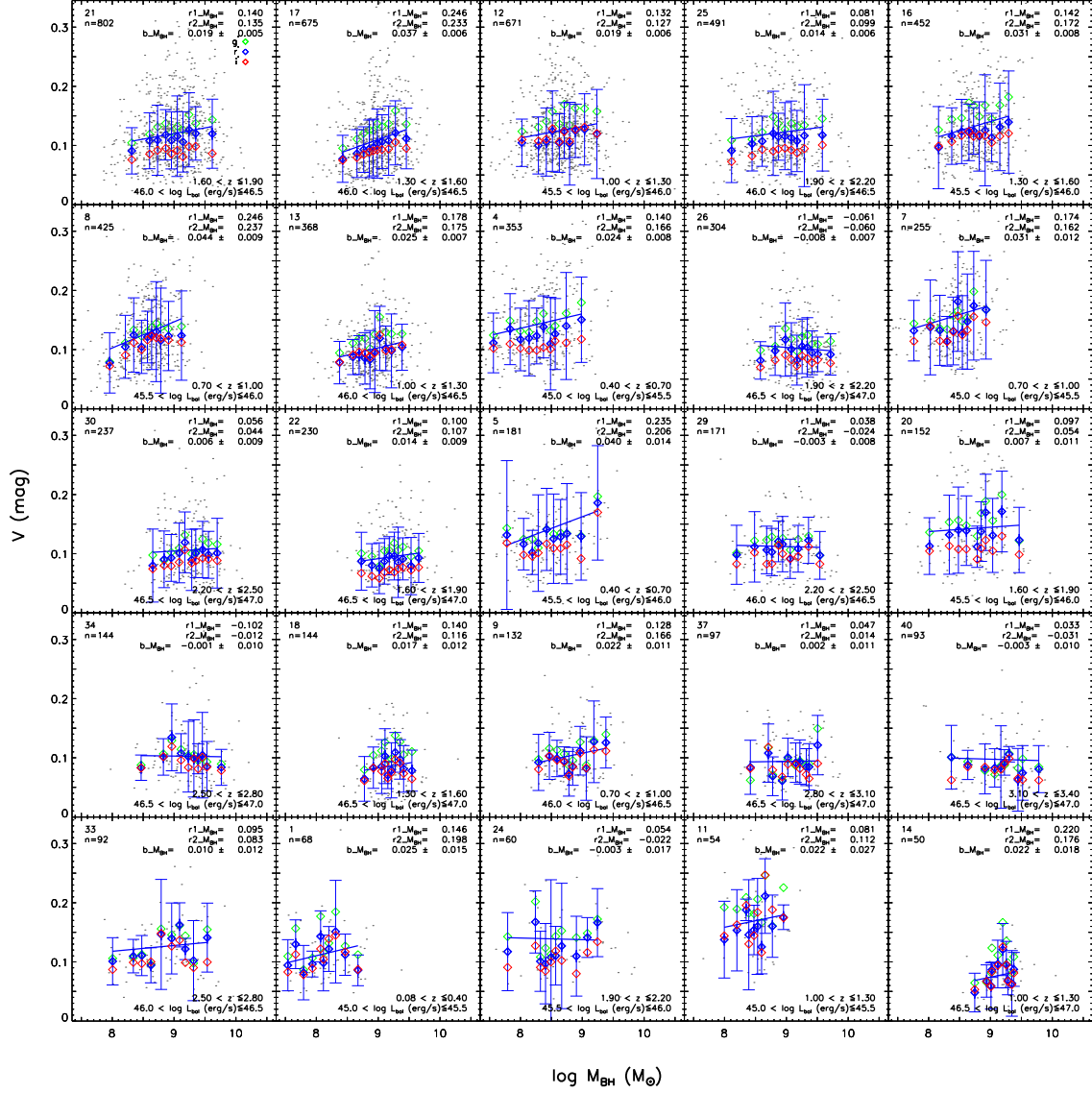


Fig. 18.— Figure similar to Fig. 17, but for the qualified subsamples obtained from the  $\log L_{\text{bol}}-z$  space as illustrated in Fig. 10. Refer to Fig. 28 in the Appendix for the radio-loud quasars.

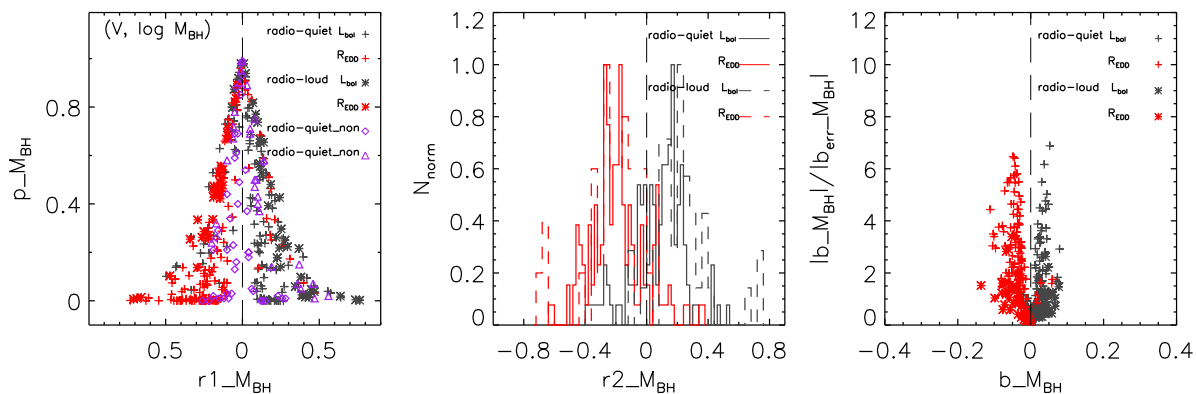


Fig. 19.— Figure similar to Fig. 13, but for the statistical results of the relationship between  $V$  and  $\log M_{\text{BH}}$ . The red signs and lines represent the results from the subsamples obtained from the  $\log R_{\text{Edd}}-z$  space and grey ones represent the results from the subsamples obtained from the  $\log L_{\text{bol}}-z$  space.

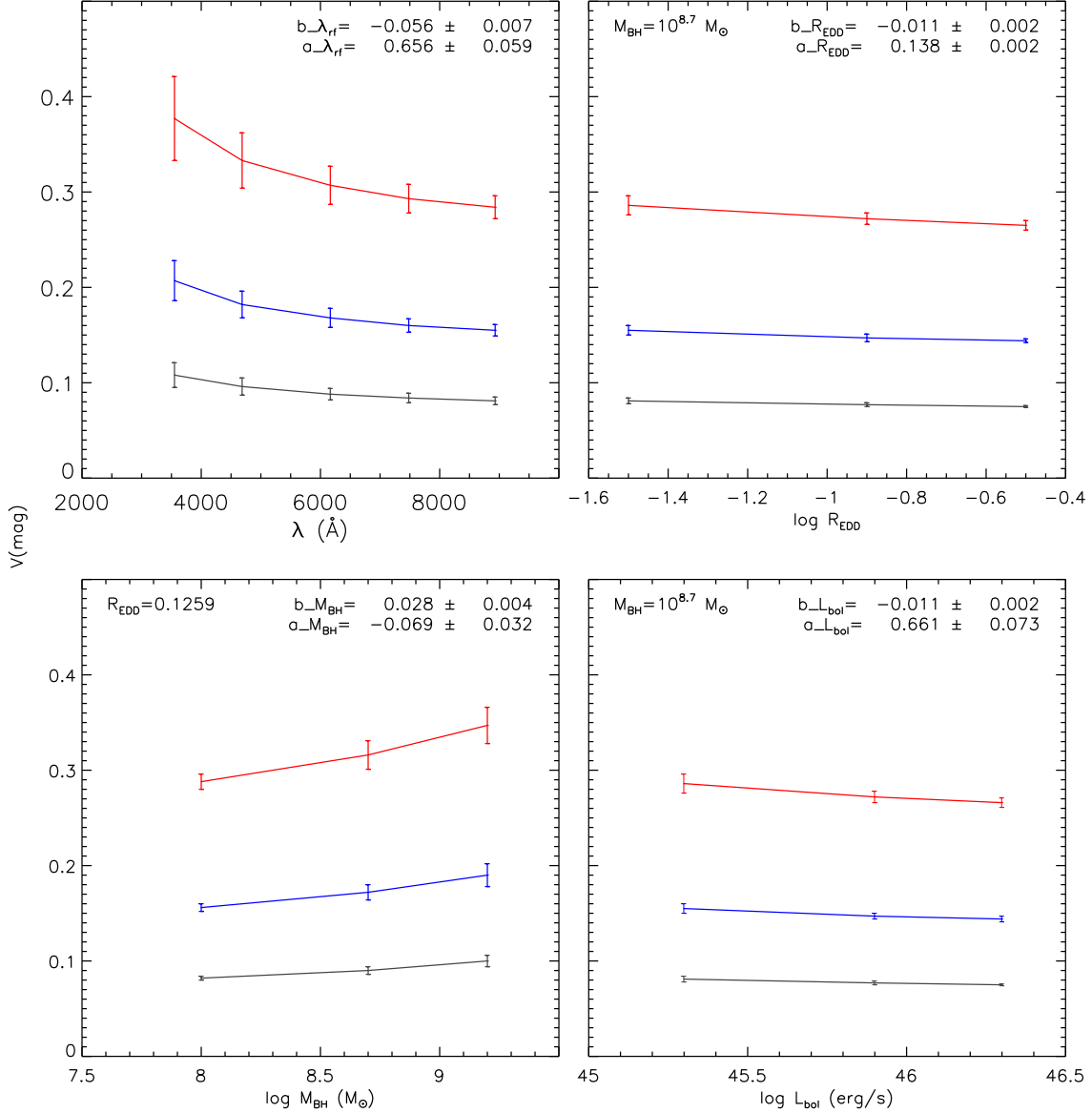


Fig. 20.— The upper left panel shows the model-predicted variability amplitude as a function of wavelength, here  $M_{\text{BH}} = 10^{8.7} M_{\odot}$  and  $R_{\text{EDD}} = 0.1259$ ; the upper right panel shows the variability amplitude in  $r'$  band as a function of  $R_{\text{EDD}}$ . The lower left panel shows the variability amplitude in the  $r'$  band as a function of  $M_{\text{BH}}$ ; the lower right panel shows the variability amplitude in the  $r'$  band as a function of  $L_{\text{bol}}$ . The red, blue and black lines refer to the cases with different changes of accretion rate, namely  $0.4\dot{m}$ ,  $0.2\dot{m}$  and  $0.1\dot{m}$ . The obtained slope  $b$  values for the simulated data during the case with the change of accretion rate at  $0.2\dot{m}$  are shown in the upper right corner of each panel.

## A. Appendix

For the radio-loud quasars, we use the same mechanism to investigate correlations between  $V$  and quasar parameters. The detailed relations are shown here.



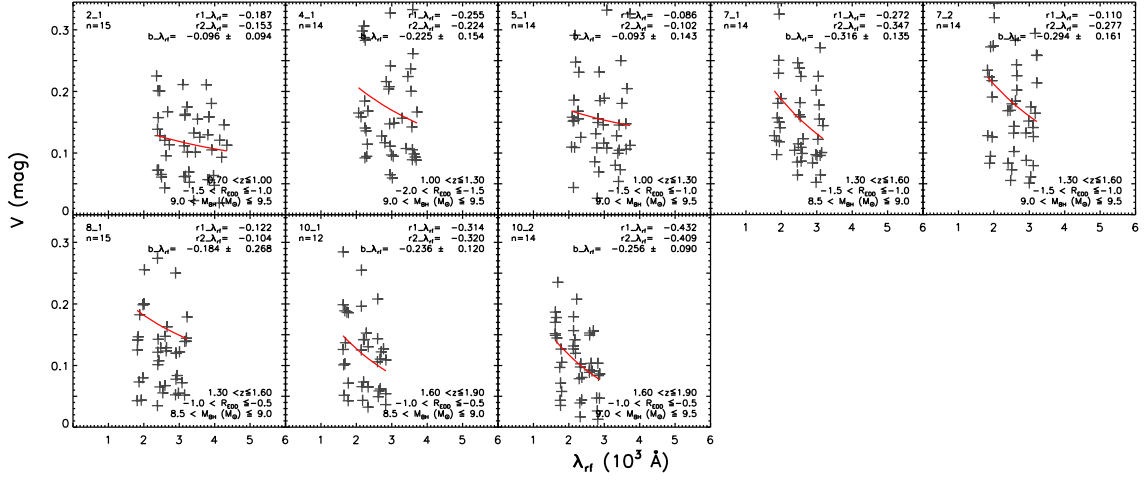


Fig. 21.— Dependence of  $V$  on  $\lambda_{rf}$  in the  $g'$ ,  $r'$  and  $i'$  band for all the 8 radio-loud subsamples within small ranges of  $R_{EDD}$ ,  $z$  and  $M_{BH}$ . In each panel, the red curve refers to the polynomial fitting with the function similar to Eq. (4), where  $X$  is  $\lambda_{rf}$ .  $r1_{\lambda_{rf}}$ ,  $r2_{\lambda_{rf}}$  and  $b_{\lambda_{rf}}$  are shown in the upper right corner and ranges of the restricted parameters are also shown in the lower right corner. Refer to Fig. 4 for the radio-quiet quasars.

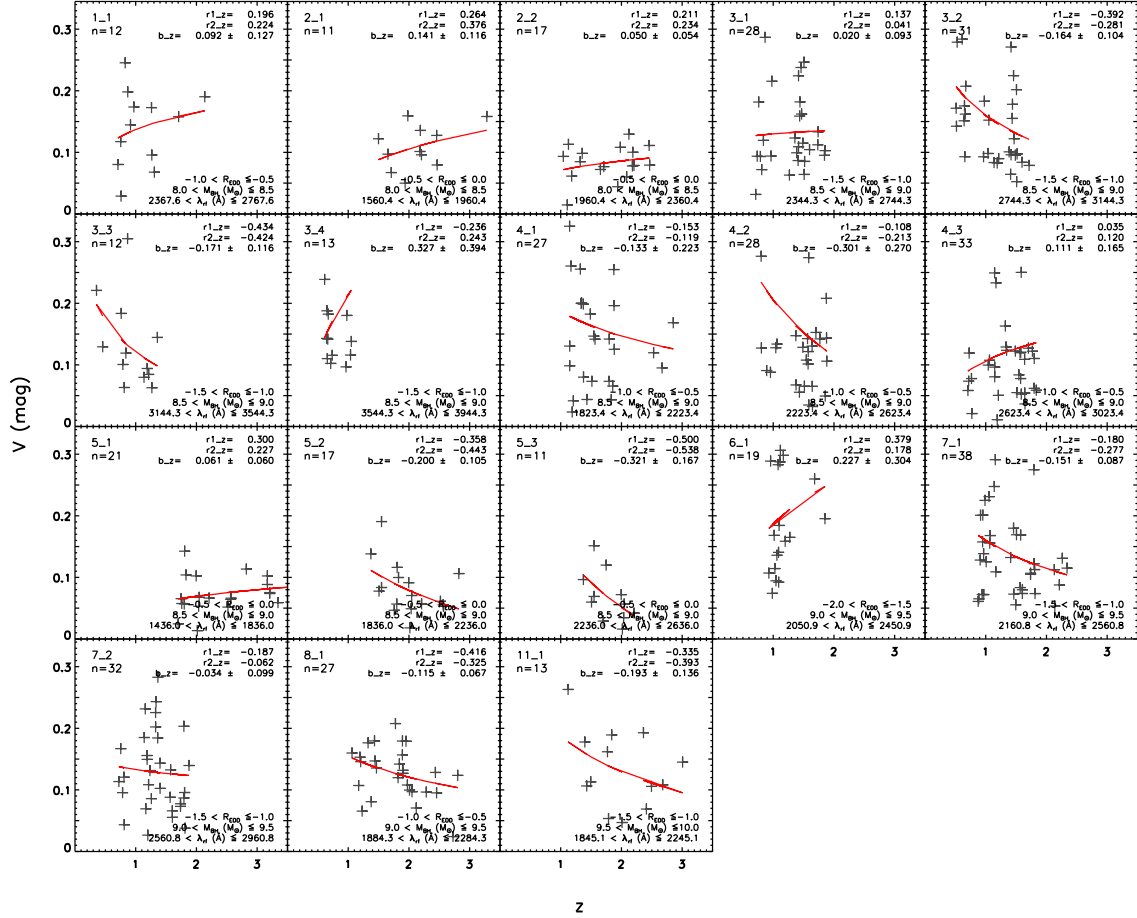


Fig. 22.— Dependence of V on z in the  $g'$ ,  $r'$  and  $i'$  band and all the 18 radio-loud subsamples within small ranges of  $R_{\text{EDD}}$ ,  $M_{\text{BH}}$  and  $\lambda_{\text{rf}}$ .  $r_{1-z}$ ,  $r_{2-z}$  and ranges of the restricted parameters are shown in the upper right corner of each panel. Refer to Fig. 7 for the radio-quiet quasars.

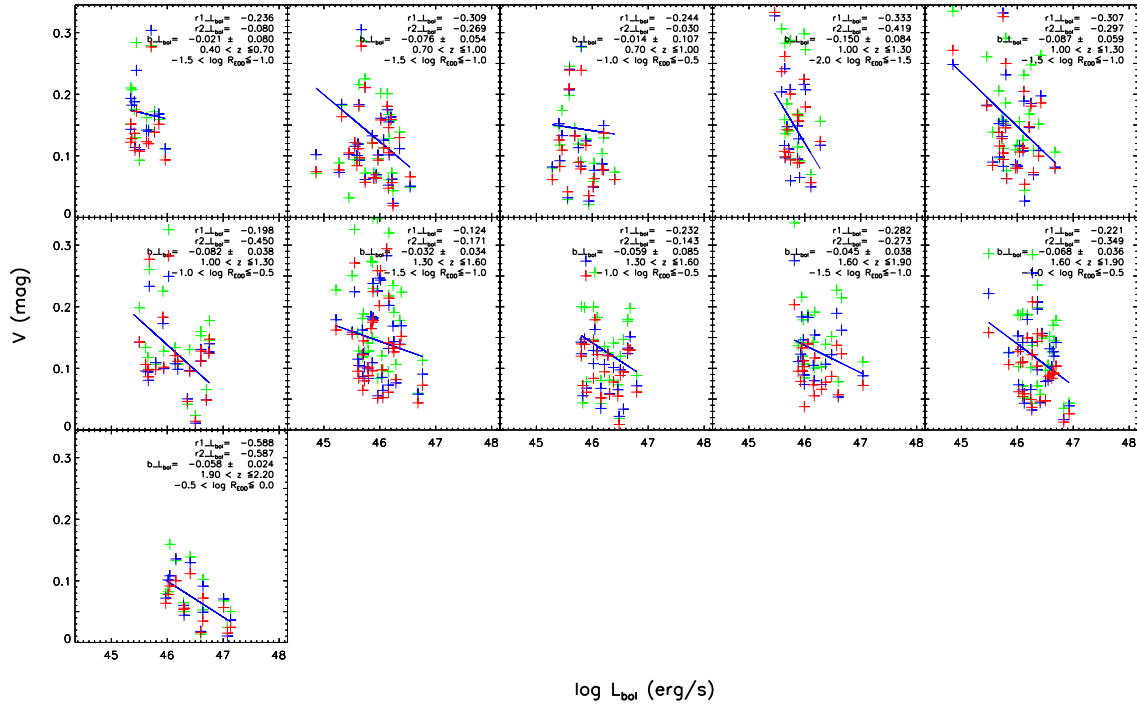


Fig. 23.— Dependence of  $V$  in the  $g'$ ,  $r'$  and  $i'$  filter band on  $L_{\text{bol}}$  in the qualified subsamples obtained from the  $\log R_{\text{EDD}}-z$  space, represented by green, blue and red plus signs respectively. The blue line refer to the linear fit for all the data in the  $r'$  band. The legends in the upper right corner of each panel refer to the  $r1-L_{\text{bol}}$ ,  $r2-L_{\text{bol}}$  and  $b-L_{\text{bol}}$  for the study of the variability amplitudes in the  $r'$  band and ranges of the restricted parameters. Refer to Fig. 11 for the radio-quiet quasars.

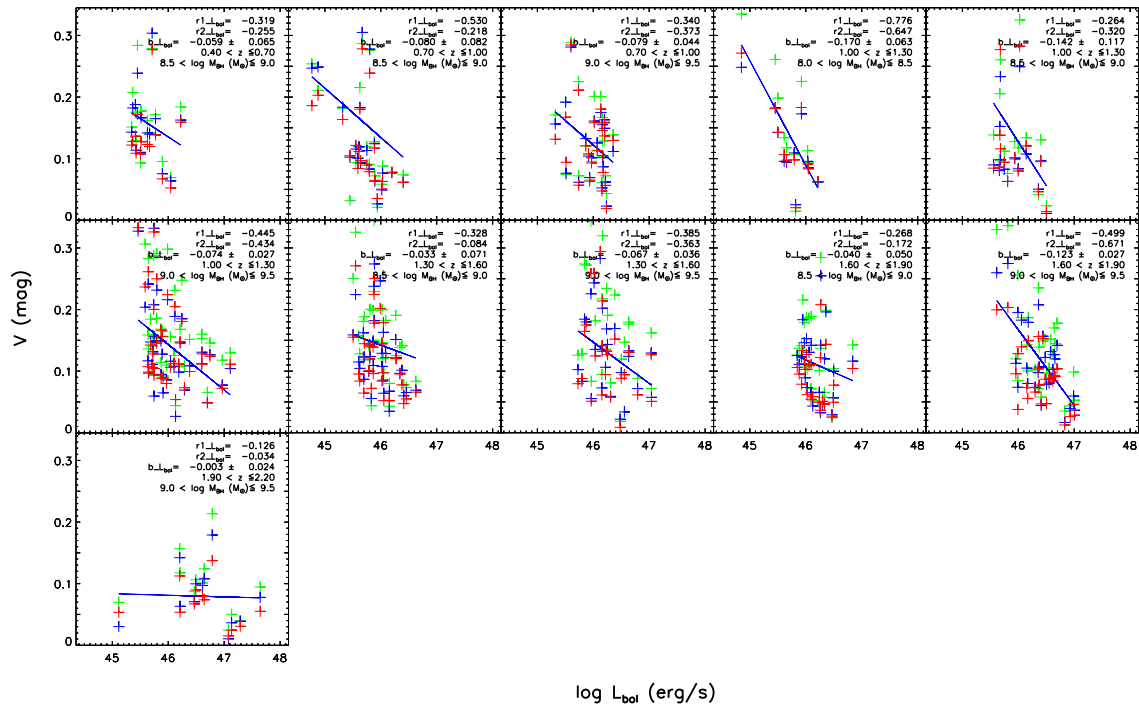


Fig. 24.— Figure similar to Fig. 23, but for the qualified subsamples obtained in the  $\log M_{\text{BH}}-z$  space. Refer to Fig. 12 for the radio-quiet quasars.

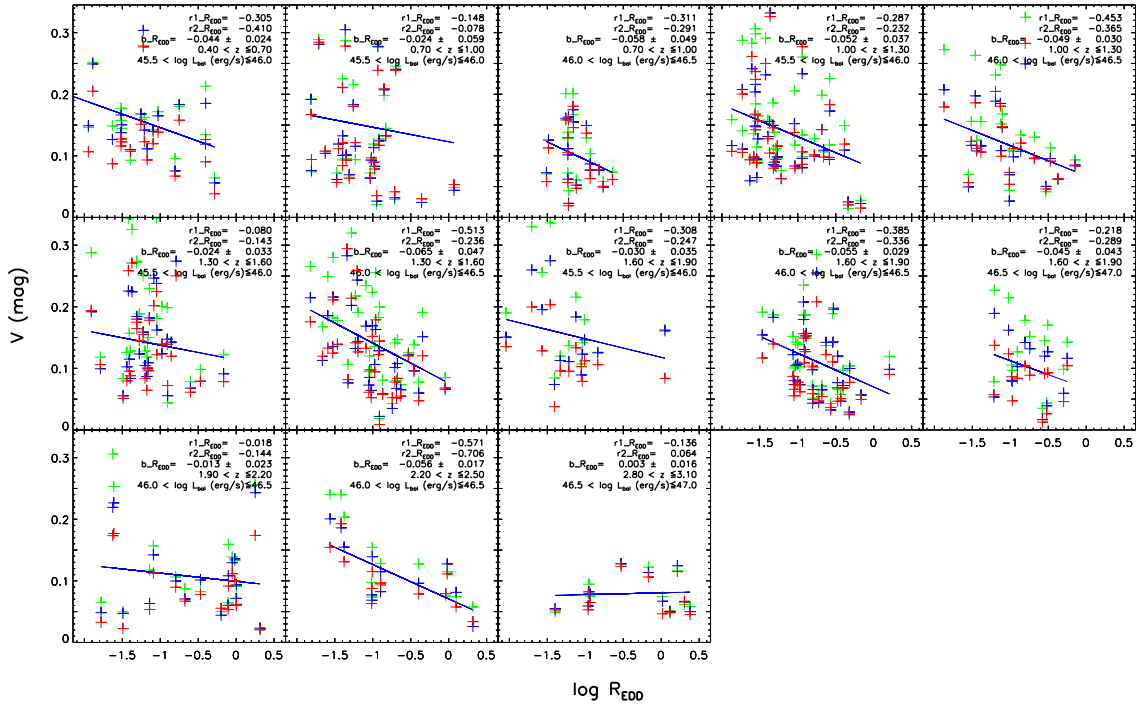


Fig. 25.— Dependence of  $V$  in the  $g'$ ,  $r'$  and  $i'$  filter band on  $R_{\text{EDD}}$  in the qualified subsamples obtained from the  $\log L_{\text{bol}}-z$  space, represented by green, blue and red plus signs respectively. The blue lines represent the linear fits for all the data in the  $r'$  band. The legends on the upper right of each panel list  $r1\_R_{\text{EDD}}$ ,  $r2\_R_{\text{EDD}}$  and  $b\_R_{\text{EDD}}$  for the study of the variability amplitudes in the  $r'$  band and ranges of the restricted parameters. Refer to Fig. 14 for the radio-quiet quasars.

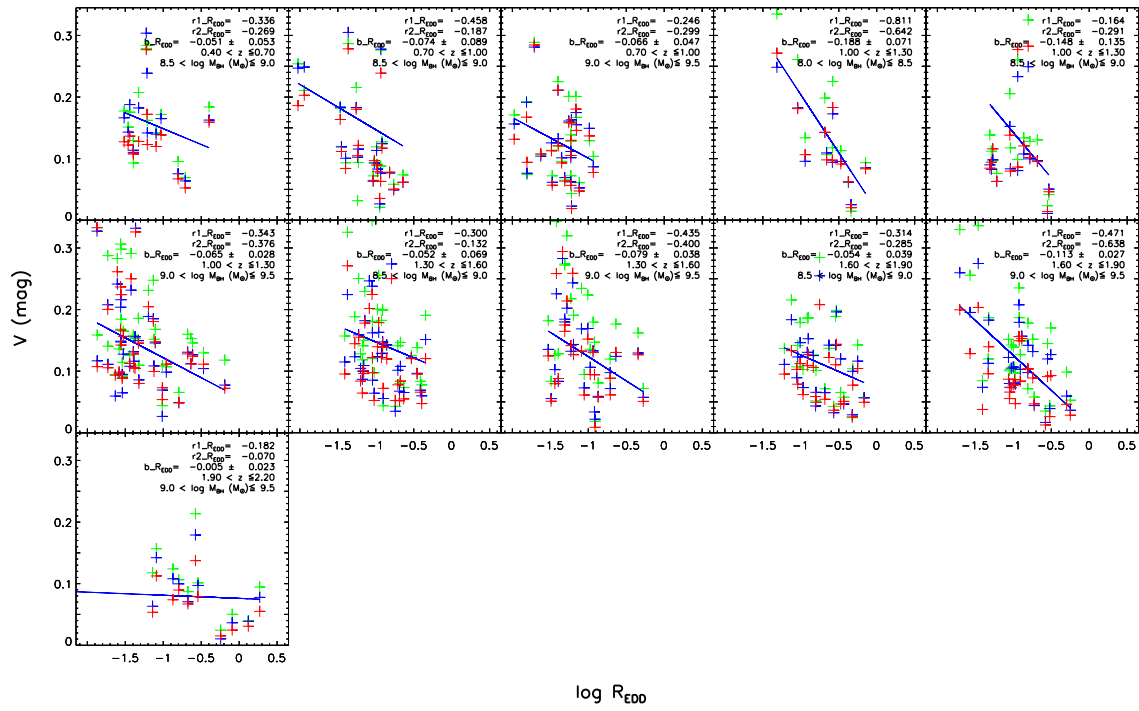


Fig. 26.— Figure similar to Fig. 25, but for the qualified subsamples obtained in the  $\log M_{\text{BH}}-z$  space. Refer to Fig. 15 for the radio-quiet quasars.

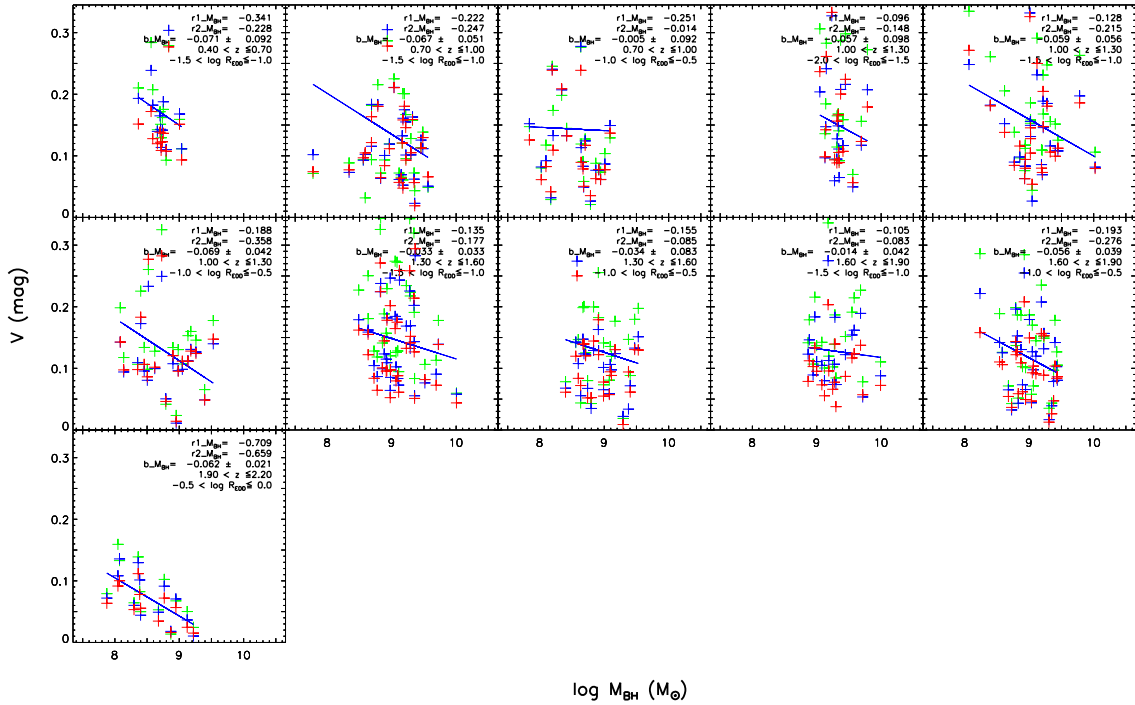


Fig. 27.— Dependence of  $V$  in the  $g'$ ,  $r'$  and  $i'$  filter band on  $M_{\text{BH}}$  in the qualified subsamples obtained from the  $\log R_{\text{EDD}}-z$  space, represented by green, blue and red plus signs respectively. The blue lines show the linear fits for all the data in the  $r'$  band. The legends on the upper right of each panel list the  $r1\_M_{\text{BH}}$ ,  $r2\_M_{\text{BH}}$  and  $b\_M_{\text{BH}}$  for the study of variability amplitude in the  $r'$  band and ranges of the restricted parameters. Refer to Fig. 17 for the radio-quiet quasars.



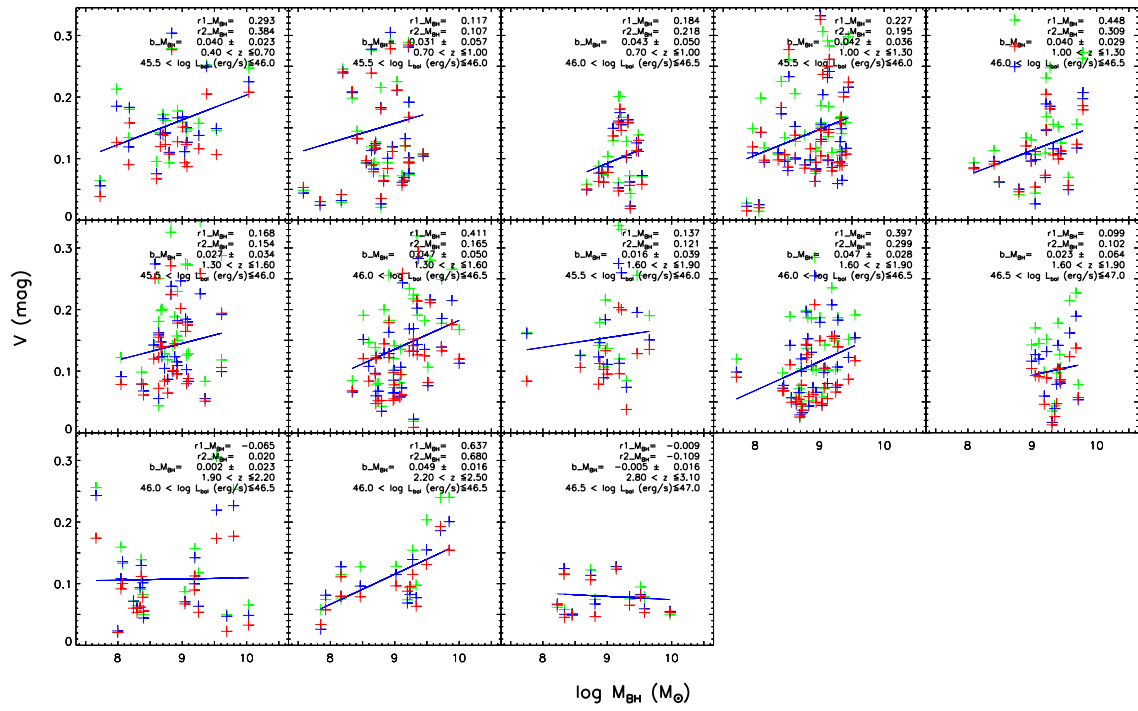


Fig. 28.— Figure similar to Fig. 27, but for the qualified subsamples obtained from the log L<sub>bol</sub>-z space. Refer to Fig. 18 for the radio-quiet quasars.